ATS Journals | American Journal of Respiratory Cell and Molecular Biology

MrgprC11+ jugular neurons control airway hyperresponsiveness in allergic airway inflammation

Journal:	*American Journal of Respiratory Cell and Molecular Biology*
Manuscript ID	Red-2024-0153OC.R1
Manuscript Type:	OC - Original Contribution
Date Submitted by the Author:	08-Aug-2024
Complete List of Authors:	Xing, Yanyan; Georgia Institute of Technology, Biological Sciences Nho, Yeseul; Georgia Institute of Technology, Biological Sciences Lawson, Katy; Georgia Institute of Technology Zhu, Yuyan; Georgia Institute of Technology Ellison, Alexandra ; Georgia Institute of Technology Chang, Margaret; Georgia Institute of Technology Hancock, William; Georgia Institute of Technology Han, Liang; Georgia Institute of Technology, Biological Sciences
Subject Category:	8.01 Airway Neural Control < INTEGRATIVE PHYSIOLOGY AND PATHOLOGY, 1.01 Airway Receptors: Nerves and Smooth Muscle < ASTHMA
Keywords:	allergic asthma, vagal sensory neurons, jugular neurons, MrgprC11, airway hyperresponsiveness, IL-4, oncostatin M, neuroimmune i

MrgprC11^{+} jugular neurons control airway hyperresponsiveness in allergic airway inflammation

Yanyan Xing, Yeseul Nho, Katy Lawson, Yuyan Zhu, Alexandra E. Ellison, Margaret Y. Chang, William Hancock, Liang Han*

School of Biological Sciences, Georgia Institute of Technology, Atlanta, GA 30332, United States

*Corresponding author: Liang Han, PhD, School of Biological Sciences, Georgia Institute of Technology, Atlanta, GA 30332, USA. Email: lhan41@gatech.edu

Author Contributions: Conceptualization: LH; Formal Analysis: YX, YN, KL, YZ, LH; Investigation: YX, YN, KL, YZ, AEE, MYC, WH, LH; Manuscript Writing : LH; Supervision: LH; Funding Acquisition: LH.

Completing Interest Statement: The authors claim no conflict of interest.

ABSTRACT

The lung is densely innervated by sensory nerves, the majority of which are derived from the vagal sensory neurons. Vagal ganglia consist of two different ganglia, termed nodose and jugular ganglia, with distinct embryonic origins, innervation patterns, and physiological functions in the periphery. Since nodose neurons constitute the majority of the vagal ganglia, our understanding of the function of jugular nerves in the lung is very limited. This study aims to investigate the role of MrgprC11$^+$ jugular sensory neurons in a mouse allergic asthma model. Our previous study has shown that MrgprC11$^+$ jugular neurons mediate cholinergic bronchoconstriction. In this study, we found that in addition to MrgprC11, several other Mrgpr family members including MrgprA3, MrgprB4, and MrgprD are also specifically expressed in the jugular sensory neurons. MrgprC11$^+$ jugular neurons exhibit dense innervation in the respiratory tract including the larynx, trachea, proximal, and distal bronchus. We also found that receptors for IL-4 and oncostatin M, two critical cytokines promoting allergic airway inflammation, are mainly expressed in jugular sensory neurons. Both IL-4 and oncostatin M can sensitize the neuronal responses of MrgprC11$^+$ jugular neurons. Moreover, ablation of MrgprC11$^+$ neurons significantly inhibited airway hyperresponsiveness in the asthmatic lung, demonstrating the critical role of MrgprC11$^+$ neurons in controlling airway constriction. Our results emphasize the critical role of jugular sensory neurons in respiratory diseases and present MrgprC11$^+$ neurons as a potential therapeutic target for treating airway hyperresponsiveness.

Key words: allergic asthma, vagal sensory neurons, jugular neurons, MrgprC11, airway hyperresponsiveness, IL-4, oncostatin M, neuroimmune interactions

INTRODUCTION

Asthma is a chronic inflammatory disease of the conducting airways and is characterized by airway inflammation, airflow obstruction due to mucus overproduction and bronchoconstiction, and airway hyperresponsiveness (AHR). Recent basic and clinical research has led to a better understanding of the immunological mechanisms of asthma. However, the neural mechanisms underlying asthma symptoms remain unclear (1-3). Recent studies showed that vagal sensory neurons contribute to asthma symptoms such as allergic inflammation, mucous cell metaplasia, and airway hyperresponsiveness (4-14).

The lung receives dense innervation from interoceptors, sensory nerves that monitor internal states, with the majority originating from vagal ganglion neurons (10, 15, 16). A mouse vagal ganglion complex is comprised of the neural crest-derived jugular ganglion occupying the rostral pole and the placode-derived nodose ganglion forming the body and caudal pole. Jugular and nodose neurons exhibit distinct transcriptional profiles, innervation patterns, and physiological functions in the peripheral. While most of the functional investigations have been focusing on nodose neurons since they constitute the majority of vagal sensory neurons (~75%), studies also showed that jugular neurons play a key role in lung interoception (15-18). However, our understanding of the physiological functions of jugular neurons in the lung are limited.

The contribution of neuroimmune interactions to asthma phenotypes has been well recognized (19). Crosson *et al* discovered that lung sensory nerves express the high-affinity IgE receptor FcεR1 and directly respond to allergen/IgE complex to initiate airway inflammation (11). Lung interoceptors in the asthmatic lung exhibit denser network and excessive activities, suggesting that allergic airway inflammation modulates neuronal activities (20-22). Several neuropeptides secreted by lung sensory nerves upon stimulation such as VIP, NMU, CGRP, and substance P have

been shown to contribute to airway inflammation, mucus hyperplasia, and airway hyperresponsiveness (AHR) (5, 7-9, 23). In addition, ablation or inhibition of sensory afferents in the airway effectively blocked asthma phenotypes, emphasizing the role of neuroimmune interactions in the pathogenesis of asthma (5, 6, 9, 12, 13). Since approaches in the previous studies are targeting all the vagal sensory nerves including jugular and nodose nerves, the specific role of jugular nerves in the neuroimmune interactions in the airway remain poorly defined.

Airway hyperresponsiveness (AHR) is the excessive narrowing of the airways due to airway smooth muscle contraction in response to various stimuli. It is a hallmark feature of multiple respiratory diseases including asthma, chronic obstructive pulmonary disease, and respiratory viral infections (24). Ample evidence demonstrated by previous studies suggest that the main cause of AHR is the remodeling of airway smooth muscle induced by inflammation (24). However, a recent study showed that acute vagotomy, a surgical procedure to cut vagus nerves, blocked AHR in asthmatic mice (14). Ablation of $TRPV1^+$ sensory neurons also abolished the AHR in asthmatic mice but did not affect the airway inflammation (12). These results suggest the neural mechanism controlling AHR can be separated from the immune components. Consistently, Su *et al* showed that Dbh^+ neurons in the nucleus of the solitary tract (nTS) of the brainstem, where the central terminals of vagal sensory neurons are projected to, are critical for AHR in asthma model (25). Ablation or chemogenetic silencing of Dbh^+ neurons blunted AHR but did not change the airway immune responses. However, since previous studies manipulated either all vagal sensory nerves by vagotomy or $TRPV1^+$ neurons which constitute more than 60% of vagal neurons, the specific vagal neuron population controlling AHR has not been molecularly identified.

The Mrgpr (mas-related G-protein coupled receptor) family comprises over 20 functional members, organized into distinct subfamilies including MrgprA1-22, MrgprB1-13, MrgprC1-14,

and MrgprD-G (26). Multiple Mrgprs are specifically expressed in sensory neurons and recent investigations demonstrated their important roles in somatosensation including pain, itch, and touch (27-35). We recently discovered that MrgprC11 is expressed in a small subset of jugular neurons innervating the airway (6). Strikingly, stimulation of MrgprC11$^+$ neurons evokes cholinergic bronchoconstriction and enhancement of airway responsiveness. Deletion of Mrgpr family members significantly reduced anaphylactic bronchoconstriction and AHR induced by influenza virus infection but did not affect airway inflammation. These results present MrgprC11$^+$ jugular neurons as a unique neuronal population controlling AHR. However, whether and how MrgprC11$^+$ jugular neurons contribute to asthma symptoms is not clear.

In this study, we first examined the expression of multiple Mrgpr family members and found that MrgprA3, MrgprB4, and MrgprD are also specifically expressed in jugular sensory neurons. The expressions of MrgprC11 and MrgprD define two distinct jugular neuron populations. We then focused our investigation on the function of MrgprC11$^+$ neurons in the airway. Using axonal tracing with genetic labeling, our data revealed dense MrgprC11$^+$ nerves throughout the respiratory tract including the larynx, trachea, proximal and distal bronchus. We also showed that receptors for IL-4 and oncostatin M, two critical cytokines for the pathogenesis of allergic asthma, are predominantly expressed in jugular neurons and both cytokines sensitize the neuronal activity of MrgprC11$^+$ neurons. Furthermore, ablation of MrgprC11$^+$ jugular neurons significantly blocked airway hyperresponsiveness in asthmatic mice without affecting the airway inflammation. Taken together, our data revealed unique neuroimmune interactions between the jugular sensory neurons and asthmatic cytokines that contribute to AHR and demonstrate the critical function of MrgprC11$^+$ jugular neurons in controlling airway constriction.

RESULTS

Mrgpr family members define unique populations of jugular nociceptors

Our previous study showed that MrgprC11 is selectively expressed in jugular sensory neurons, but not in nodose sensory neurons (6). To investigate the function of Mrgprs in interoception, we here examined if other Mrgpr family members are expressed in vagal sensory neurons using genetic labeling (Figure 1). The mouse lines we have used include *MrgprA3$^{Cre\text{-}EGFP}$; ROSA26^{tdTomato} (MrgprA3^{tdTomato}), MrgprC11^{CreER}; ROSA26^{tdTomato} (MrgprC11^{tdTomato}), MrgprB4^{PLAP},* and *MrgprD^{CreER};ROSA26^{PLAP} (MrgprD^{PLAP}).* TdTomato and alkaline phosphatase (PLAP: human placental alkaline phosphatase) were used as neuronal tracers in this experiment (Figure S1 A-D). Alkaline phosphatase can generate strong purple to blue color in a whole mount histochemistry preparation and the results can be easily visualized with a dissecting microscope (36). Consistent with previous reports (29, 30, 34, 37, 38), we have observed expression of these four Mrgprs in DRGs and Mrgprs^{+} cell bodies are evenly distributed within the DRGs. We found that all four Mrgprs are also expressed in subsets of vagal sensory neurons. Interestingly, all Mrgprs^{+} vagal sensory neurons are located in the rostral part of the ganglia, suggesting that they are selectively expressed in jugular neurons (Figure 1 A-D).

Cre-dependent labeling might label cells that only transiently express the Mrgprs genes during development. To confirm the expression of these four Mrgprs in jugular neurons in adult mice, we performed RNAscope *in situ* hybridization with probes targeting Mrgprs and Prdm12, a marker for jugular sensory neurons (Figure 1E). All four Mrgprs are only expressed in Prdm12^{+} neurons, demonstrating that they are jugular specific. Each mouse vagal ganglia contains ~2,300 neurons and about 25% of them are jugular neurons (~575 neurons per ganglion). The expressions of MrgprA3 and MrgprB4 are sparse and constitute about 1.32% (41/1,606, ~7-8 neurons per ganglion) and 3.61% (60/1,660, ~20 neurons per ganglion) jugular neurons respectively.

Approximately 20.3% of jugular neurons are expressing MrgprC11 (226/1113, ~ 117 neurons per ganglion) and 37.3% of jugular neurons are expressing MrgprD (461/1236, ~214 neurons per ganglion) (Figure 1G). The expressions of MrgprC11 and MrgprD are non-overlapping (Figure 1F), demonstrating that they define two distinct jugular nociceptive populations. The current study is focusing on the function of MrgprC11^{+} jugular neurons in the lung.

Innervation pattern of MrgprC11^{+} jugular neurons in the airway

Our previous study using retrograde tracing with CTB488 demonstrated that MrgprC11^{+} jugular neurons innervate the airway (6). However, which location(s) in the airway those sensory nerves terminate and how the MrgprC11^{+} terminal arbors look have never been investigated. Here, we used *MrgprC11^{PLAP}* mice and alkaline phosphatase axonal tracer to visualize the nerves in the airway (Figure 2). MrgprC11^{+} innervations were observed in the larynx region, trachea, and the lung. The nerve density in the larynx region is high, indicating an undiscovered function of MrgprC11^{+} neurons in the larynx (Figure 2A). In the trachea, MrgprC11^{+} nerves run parallel to the cartilages and form plexuses in the trachealis muscle (Figure 2B). This result is consistent with previous studies showing jugular innervations in the trachea in mice.

We also observed dense MrgprC11^{+} nerves throughout the bronchial tree. Sensory nerves in the peripheral organs always overlap and intermingle, making it harder to examine the morphology of the innervation pattern of individual neurons. To better visualize the MrgprC11^{+} sensory arbors in the lung, we administered a low dose tamoxifen (10mg/kg, once) to only activate CreER in a small subset of CreER^{+} cells (Figure 2D-E). This sparse labeling technique will not change the specificity of the Cre-dependent labeling and has been widely used to examine the neuronal morphology (39, 40). Our group has recently used the same strategy to visualize individual MrgprC11^{+} sensory arbors in the skin and the spinal cord (36, 41). MgprC11^{+} nerves inside of the

lung exhibit free-nerve endings (Figure 2D-E). Terminal arbors were observed in both proximal large airway (Figure 2D) and the distal small airway (Figure 2E). Lung sections isolated from *MrgprC11*^{tdTomato} mice showed that MrgprC11^{+} nerves penetrate into the superficial luminal surface, allowing them to directly sense airway irritation (Figure 2F). This is consistent with the fact that MrgprC11^{+} jugular sensory neurons are nociceptors (6).

The airway is innervated by sensory nerves derived from both vagal ganglia and DRG, although previous studies showed that the majority of innervations in the airway are derived from vagal ganglia (10, 15, 16, 42). To confirm the airway innervation of MrgprC11^{+} jugular sensory neurons, we injected Cre-dependent AAV-flex-tdTomato directly to the vagal ganglia of *MrgprC11*^{CreER} mice. The mice were treated with tamoxifen 5 days after the AAV injection (75 mg/ml, i.p., 5 consecutive days) and the vagal ganglia and lung were collected for examination 6 weeks after the AAV injection (Figure 3A-C). Cre-independent AAV-EGFP was co-injected and both jugular and nodose neurons are expressing EGFP (Figure 3B&C). However, tdTomato is only expressed in the MrgprC11^{+} jugular neurons in the rostral part of the ganglia (Figure 3D). Lung sections collected from the AAV-injected *MrgprC11*^{CreER} mice showed tdTomato^{+} nerves in the lung (Figure 3E), demonstrating that MrgprC11^{+} jugular sensory neurons innervate the lung.

Neuroimmune interactions between the MrgprC11^{+} neurons and the inflamed lung

To understand the neuroimmune interactions between MrgprC11^{+} lung interoceptive nerves and the inflamed lung, we analyzed the previous transcriptomic datasets of vagal sensory neurons to examine if MrgprC11^{+} jugular neurons express any cytokine receptors (18, 43-46). We found two candidate genes that might play a role in the neuroimmune interactions between jugular sensory nerves and the inflamed lung: IL-4 receptor alpha (IL4ra) and oncostatin M receptor (OSMR). Our RNAscope *in situ* analysis showed that IL4ra is predominantly expressed in jugular neurons (Fig.

4A, 4A', 4A"). 79.1% (407/570) of IL4ra$^+$ neurons are Prdm12$^+$. The fluorescent intensity of *in situ* signals in IL4ra$^+$ jugular cells are much higher compared to those in IL4ra$^+$ nodose neurons, suggesting that the expression level of IL4ra is higher in jugular neurons (Figure 4B). The majority of MrgprC11$^+$ neurons (71.3%, 92/129) are expressing Il4ra, indicating the interaction between IL-4 and MrgprC11$^+$ neurons (Figure 4C).

A previous study has shown that IL-4 sensitized the responses of DRG sensory neurons to pruritogens and promote chronic itch (47). To examine if IL-4 interact with lung interoceptors, we performed calcium imaging analysis of vagal sensory neurons isolated from *Pirt*^{GCaMP3} mice, in which sensory neurons are expressing GCaMP3 (48). We found that IL4 rarely activates vagal sensory neurons directly. 6 coverslips (totally 668 sensory neurons on the coverslips) from two different batches of cell culture were tested and only one cell (0.15%) showed increased GCaMP3 fluorescence level upon IL4 stimulation. However, IL-4 sensitized the responses of MrgprC11$^+$ neurons to Bam8-22 (Figure 4 D-E). We exposed vagal sensory neurons to Bam8-22 (100 nM) both before and after IL-4 (300 nM, 3min) treatment. Subthreshold concentration of Bam8-22 (100 nM) normally does not effectively activate vagal sensory neurons. However, IL-4 treatment increased the percentage of Bam8-22-responsive neurons from 1.02% ± 0.30% to 3.13% ± 0.90% (Figure 4E). Therefore, our findings suggest that IL-4 sensitizes the neuronal responses of MrgprC11$^+$ neurons. To rule out the possibility that the initial exposure to Bam8-22 can prime the response to subsequent Bam8-22 application, we have challenged the neurons with Bam8-22, followed by calcium imaging buffer, and then with Bam8-22 again. The proportions of Bam-responsive vagal sensory neurons were similar before and after the calcium imaging buffer incubation (Figure 4F), suggesting that the initial Bam8-22 challenge did not sensitize the following neuronal responses.

Oncostatin M (OSM) was demonstrated to be a critical cytokine for allergic airway inflammation recently (49-53). It has been shown that OSM enhances the neural excitability of itch-sensing cutaneous nerves and promotes chronic itch (54). Therefore, we here examine if OSM interacts with lung interoceptors. RNAscope *in situ* analysis demonstrated that OSMR is only expressed in Prdm12$^+$ jugular neurons and OSMR$^+$ neurons constitute about 15.1% (67/443) of jugular neurons (Figure 5A). More than half of MrgprC11$^+$ neurons (58%, 94/162) also express OSMR (Figure 5B). Surprisingly, we found that gp130 is also predominantly expressed in jugular neurons (96%, 244/254) (Figure 5A). Gp130 is the common co-receptor for the nine interleukin-6 family cytokines including OSM, most of which have been implicated in the inflammatory lung diseases (55). This result indicates that jugular neurons, not nodose neurons, play a key role in the neuroimmune interactions between the IL-6 family and the inflamed lung. The result highlights the critical function of jugular neurons in respiratory disease and the physiological differences between jugular and nodose.

Consistent with previous reports (49-53), our real-time PCR analysis showed increased OSM expression in the asthmatic lung (Figure 5C). Similar to IL-4, OSM rarely directly activates vagal sensory neurons. Interestingly, OSM also sensitized the responses of MrgprC11$^+$ neurons to Bam8-22 (Figure 5D-E). Take together, our findings suggest that both IL-4 and OSM, two critical cytokines for airway allergic inflammation, sensitized the neuronal responses of MrgprC11$^+$ neurons.

We next examined if the allergic inflammation alters the expression of IL4ra and OSMR in the vagal sensory neurons in inflamed mice. OSMR expression is restricted to jugular neurons in naïve mice (Figure 5A). In inflamed mice, we detected a limited number of OSMR$^+$ neurons that did not express Prdm12 (5/612 in 6 mice), suggesting that allergic airway inflammation may induce

OSMR expression in nodose neurons, although the effect appears minimal. We did not observe a significant change of the percentage of OSMR$^+$ neurons in jugular after OVA treatments (Figure S1A-B), although qPCR analysis of the vagal ganglia showed a decrease of OSMR expression in the inflamed mice (Figure S1C). IL4ra is expressed in both jugular and nodose neurons, with the majority of IL4ra$^+$ neurons (~80%) in jugular. We performed both RNAscope *in situ* of vagal ganglia sections and qPCR analysis of vagal ganglia and did not detect any changes of the IL4ra expression after OVA treatments (Figure S2).

Sensitized responses of MrgprC11$^+$ jugular sensory neurons in the mouse allergic asthma model

We next examined how airway inflammation modulates the activities of MrgprC11$^+$ jugular neurons. We found that MrgprC11 expression is still restricted to jugular neurons in the OVA-treated mice (Figure 6A), suggesting that the allergic airway inflammation did not induce the expression of MrgprC11 expression in nodose neurons. The allergic airway inflammation increased the expression of MrgprC11 in jugular neurons. Both the MrgprC11 mRNA level (Figure 6C) and the percentage of MrgprC11$^+$ neurons in jugular (Figure 6B) were increased significantly. Consistently, bronchoconstriction induced by Bam8-22, a specific agonist of MrgprC11 (6), was also significantly increased in the inflamed mice (Figure 6C). A subthreshold concentration of Bam8-22 that only induced a small change in the naïve mice triggered a significant increase of lung resistance (R_L) in inflamed mice. We also examined if airway inflammation generates any endogenous agonists for MrgprC11$^+$ nerves. We performed real-time PCR to detect the expression of cathepsin S, a previously identified MrgprC11 agonist. Consistent with previous reports (56, 57), we found that the expression of cathepsin S is significantly increased in the inflamed lung (Figure 6D), suggesting potential interactions between cathepsin S and MrgprC11$^+$ neurons in the

inflamed lung. In summary, these data suggest that airway allergic inflammation sensitizes MrgprC11^{+} jugular neurons.

Previous studies have demonstrated the important role of TRPV1^{+} vagal sensory neurons in airway hyperresponsiveness (11, 12, 58), we here examined the expression of MrgprC11 in TRPV1^{+} neurons (Figure S3). In naïve mice, we found that the majority of MrgprC11^{+} neurons co-express TRPV1 (76.0%, 136/179), while approximately 13.4% (136/1014) of TRPV1^{+} neurons express MrgprC11 (Figure S3A). After the OVA treatments, the proportion of TRPV1^{+} neurons expressing MrgprC11 is increased, consistent with the increased expression of MrgprC11 in jugular ganglia. We did not observe changes in TRPV1 expression in MrgprC11^{+} neurons.

Ablation of MrgprC11^{+} jugular sensory neurons blocked airway hyperresponsiveness in asthmatic mice

We next generated *MrgprC11^{DTR}* mice to examine if ablation of MrgprC11^{+} neurons can reduce asthma phenotypes. 80% of MrgprC11^{+} jugular neurons were lost 4 weeks after DTX treatments (5.8% ± 0.43% vs 1.17% ± 0.25%) (Figure 7A-B). Both the *MrgprC11^{DTR}* mice and littermate control *ROSA26^{DTR}* mice developed a robust immune reaction with increased IL-4 and IL-5, decreased IFN-γ, and lung infiltration of macrophages, eosinophiles, neutrophiles, and lymphocytes (Figure 7C-F), suggesting that MrgprC11^{+} neurons are not required for allergic airway inflammation. The *ROSA26^{DTR}* mice developed AHR after the OVA treatments evidenced by the significantly increased airway resistance in response to methacholine challenges. However, we found that the ablated mice showed significantly decreased AHR compared to control mice (Figure 7G-H), suggesting that MrgprC11^{+} neurons are required for AHR in asthmatic mice.

DISCUSSION

Jugular sensory neurons play critical physiological roles in multiple internal organs in health and diseases (59). The sparsity of these neurons and the lack of molecular labeling, however, limited the depth of understanding regarding their specific functions. In this study, our mouse transgenic tools allow us to reveal the specific expression of Mrgpr family members including MrgprA3, MgprB4, MrgprC11, and MrgprD in jugular sensory neurons and investigate the function of MrgprC11$^+$ jugular neurons in allergic asthma. Cre-dependent axonal tracing demonstrate extensive innervation by MrgprC11$^+$ nerves throughout the bronchial tree. Our data show that allergic inflammation in the airway changes the physiological properties of MrgprC11$^+$ neurons by upregulating the expression of MrgprC11 and sensitizing the neuronal responses of MrgprC11$^+$ neurons. We further identified two cytokines, IL-4 and OSM, that contribute to the sensitization of MrgprC11$^+$ neurons. Receptors of both cytokines are predominantly expressed in jugular sensory neurons in the vagal ganglia and promote calcium responses of MrgprC11$^+$ neurons to agonist Bam8-22. In addition, cathepsin S, a MrgprC11 agonist, is highly expressed in the inflamed airway, indicating continuous activation of MrgprC11$^+$ jugular neurons during airway inflammation. Moreover, ablation of MrgprC11$^+$ neurons diminished AHR in asthmatic mice, demonstrating the essential role these neurons play in controlling airway constriction. These results demonstrate novel neuroimmune interactions between jugular sensory neurons and the asthmatic lung and highlight the essential role of jugular sensory neurons in allergic asthma.

Transcriptomic analyses of vagal sensory neurons have been reported by multiple groups and the transcriptional profiles of more than 30 clusters of nodose neurons have been identified (18, 43-46). However, available transcriptomic analysis of jugular neurons is still limited due to the sparsity of the jugular neurons and their low survival rate during dissociation. Single cell profiling by Kupari *et al.* has identified six clusters of jugular neurons, however the expression of MrgprC11

was not detected (43). Our identification of MrgprC11, OSMR, and IL4ra in the jugular neurons is consistent with the report by Liu et al. which performed single-cell sequencing of airway-innervating vagal sensory neurons. But only one jugular nociceptive cluster with 15 neurons was identified in the study (44). Using Cre-mediated genetic labeling, our results presented four jugular C-fiber populations including MrgprA3$^+$, MrgprB4$^+$, MrgprC11$^+$, and MrgprD$^+$ neurons. Although our previous (6) and current studies demonstrate the critical role of MrgprC11$^+$ neurons in controlling airway constriction, the peripheral innervation targets and functions of the other three neuronal populations remain unknown. Future studies investigating these jugular populations will improve our understanding of interoceptive nerves and how they contribute to the physiological functions of internal organs.

Although both nodose and jugular neurons innervate the conducting airway throughout the lung, the two sensory ganglia exhibit distinct innervation patterns. Previous studies in guinea pigs and rats indicate that the extrapulmonary airways including the larynx, trachea, and main bronchi are mainly innervated by jugular neurons, while the intrapulmonary airways are mainly innervated by nodose neurons (60-62). However, recent analysis by Moe et al revealed a distinct tracheal innervation pattern in mice (63). Their results showed that although mouse trachea receives innervations from both jugular and nodose neurons, the majority of the tracheal nerves are derived from autonomic and nodose neurons. Using *MrgprC11^{PLAP}* mice, we have observed MrgprC11$^+$ nerves throughout the airway tract including the larynx and trachea (Figure 2). It is unknown whether *MrgprC11^{PLAP}* mice line labels any autonomic neurons and the possibility remains that the observed PLAP$^+$ nerves originate from autonomic neurons. Although the genetic labeling induces PLAP expression in both DRG and vagal sensory neurons, it is unlikely that the observed nerves are from DRG neurons since our previous study using retrograde tracer cholera toxin B

(CTB) demonstrated that MrgprC11^{+} DRG sensory neurons do not innervate the airway (6). To provide direct evidence of MrgprC11^{+} innervation in the airway, we injected AAV-flex-tdTomato into the vagal ganglia of *MrgprC11^{CreER}* mice and the results demonstrated the innervation of MrgprC11^{+} jugular neurons in the lung.

Our results demonstrate neuroimmune interactions between MrgprC11^{+} nerves and IL-4 and OSM, two well characterized asthmatic cytokines that play critical roles in airway allergic inflammation (52, 53, 64, 65). IL-4 is a well characterized asthmatic cytokine and has been used as a biomarker for allergic asthma (64, 65). It is a typical Th2-cell-associated cytokine secreted by many immune cells participating in ongoing allergic airway inflammation such as Th2 lymphocytes, basophils, eosinophils and mast cells. IL-4 signals through the type 1 IL-4Rα/γ or the type 2 IL-4Rα/IL-13Rα receptor complexes and the functional role of IL-4 in promoting airway inflammation has been well studied (64, 65). We here show that IL-4 interact with jugular nerves and sensitize neuronal activities of MrgprC11^{+} neurons to promote AHR, revealing a novel function of IL-4 in allergic respiratory disorders.

Oncostatin M (OSM) is a member of the interleukin-6 family cytokines (66). OSM exerts its function through receptor dimers gp130/OSMR or gp130/LIFR. Although elevated OSM is frequently detected in airway diseases including allergic asthma (49-51), the critical pathogenic role of OSM in asthma was only demonstrated recently (52, 53). Recent studies with mouse allergic asthma model demonstrated that OSM is necessary and sufficient to drive the allergic inflammation and OSM neutralizing antibodies attenuated both airway inflammation and AHR (52, 53). However, whether and how OSM interacts with lung interoceptors and contributes to AHR has not been reported yet. Interestingly, the expression of OSM is much higher in the lower airway of asthmatic patients with irreversible airflow obstruction than compared to the patients

without irreversible airflow obstruction, suggesting the role of OSM controlling airway constriction (51). Consistently, our data suggest that OSM can sensitize MrgprC11^{+} neurons to promote AHR in asthmatic mice. The fact that both IL-4 and OSM predominantly interact with jugular neurons, not nodose neurons, also suggests the critical role of the neuroimmune interaction between jugular nerves and inflamed airway in the pathogenesis of asthma.

Peripheral pathological conditions can remarkably affect cellular function of the innervating sensory nerves through the regulation of chromatin accessibility and gene expression. Indeed, our results showed that airway inflammation changed the expression levels of MrgprC11 and OSMR in vagal sensory neurons. We observed an upregulation of MrgprC11, which correlates with the heightened sensitivity of MrgprC11^{+}. Quantitative PCR analysis of vagal ganglia suggested a downregulation of OSMR was downregulated in vagal sensory neurons in response to airway inflammation and the elevated OSM level in the lung. This could potentially be due to a feedback mechanism to minimize neuronal responses to the increased OSM. Future studies investigating transcriptomic changes of MrgprC11^{+} lung interoceptors would provide valuable information about neural mechanisms of asthma.

Previous studies have demonstrated the critical role of lung nociceptor in the development of AHR, while conflicting evidence have been presented related to whether lung nociceptors contribute to airway allergic inflammation. Trankner et al showed that ablation of TRPV1^{+} vagal neurons abolished AHR but did not affect airway inflammation in a mouse allergic asthma model (12), suggesting that lung nociceptors do not contribute to airway inflammation. However, later studies showed that ablation of either NaV1.8^{+} or TRPV1^{+} neurons significantly reduced airway inflammation (9, 58). Indeed, TRPV1^{+} nociceptive nerves express the high-affinity IgE receptor FcεR1 and directly respond to allergen/IgE complex to initiate airway inflammation (11). In

addition, neuropeptides including CGRP, substance P, and vasoactive intestinal peptide that released by nociceptors upon stimulation also trigger airway inflammation (5, 9, 11, 58). MrgprC11$^+$ jugular neurons have significant overlap with TRPV1$^+$ vagal sensory neurons and our results showed that ablation of MrgprC11$^+$ neurons, approximately 6% of vagal sensory neurons, did not affect the airway allergic inflammation. This finding does not exclude the possibility that MrgprC11$^+$ lung interoceptors may also contribute to airway inflammation; however, the ablation of this small neuronal population did not produce a substantial effect detectable by our experimental approaches.

Our results demonstrated that the ablation of MrgprC11$^+$ jugular neurons blocked AHR. It is intriguing that ablation of such a small neuronal population (~117 neurons per ganglion) could induce significant effects in AHR. These results emphasize the important role of jugular sensory neurons in allergic asthma and suggest MrgprC11$^+$ neurons as a potential therapeutic target controlling AHR. Future studies delineating the molecular signaling pathways involved in the sensitization of these neurons by IL-4 and oncostatin M could also provide novel insights into asthma therapy.

Vagal sensory neurons project their central axons to the brain stem, and our current understanding of the central neural circuits contributing to asthma phenotypes remains limited. Previous studies have shown that airway-innervating jugular and nodose neurons exhibit distinct patterns of central innervation, with jugular neurons primarily project to the paratrigeminal nucleus (Pa5) and nodose neurons predominantly innervate the nucleus of the solitary tract (nTS) (60, 62, 67). However, contradicting results by Kim et al indicated that the majority of the jugular afferents, labeled by Tac1-Cre mouse line, terminate in the nTS (42). Nonetheless, it will be important to examine the central innervation of MrgprC11$^+$ jugular neurons in the future to better understand the neural

mechanisms underlying AHR. A recent study demonstrated that ablation or chemogenetic silencing of Dbh$^+$ neurons in the nTS abolished AHR, suggesting that Dbh$^+$ neurons are required for AHR (25). It will also be interesting to investigate the potential interaction between MrgprC11$^+$ central nerves with Dbh$^+$ neurons.

MATERIALS AND METHODS

Mice

All experiments were performed with approval from the Georgia Institute of Technology Animal Use and Care Committee. All transgenic mice used for these experiments have been backcrossed to C57BL/6 mice for at least 10 generations. All experiments were conducted using 2-4 months old (20-30g) mice, except mice used for Ca^{2+} imaging assays, which were 3-6 weeks old. Mice were housed in a vivarium with a 12-hr light/dark cycle, housing groups of 5 maximum, and food/water *ad libitum*.

Table 1. List of mouse lines

Mouse lines	Description and references	Application
Wildtype C57BL/6	Jax 000664	
ROSA26^{tdTomato}	Cre reporter line. Jax 007909	
ROSA26^{PLAP}	Cre reporter line. Jax 009253	
ROSA26^{DTR}	Cre reporter line. Jax 007900	
Pirt$^{GCaMP3/+}$	knock-in line, GCaMP3 expression controlled by the pan-sensory neuron promoter Pirt (48).	to monitor calcium mobilization in sensory neurons.
MrgprA3$^{Cre-EGFP}$	BAC transgenic line, Cre-EGFP expression controlled by MrgprA3 promoter (28).	to introduce Cre-dependent reporters in MrgprA3$^+$ neurons.
MrgprC11^{CreER}	BAC transgenic line, CreER expression controlled by MrgprC11 promoter (36).	to introduce Cre-dependent reporters in MrgprC11$^+$ neurons after tamoxifen treatment.
MrgprD^{CreER}	Knockin line, CreER expression controlled by MrgprD promoter (68). Jax 031286	to introduce Cre-dependent reporters in MrgprD$^+$ neurons after tamoxifen treatment.
MrgprB4^{PLAP}	Knockin line, PLAP expression controlled by MrgprB4 promoter (30).	to use PLAP axonal tracer to visualize MrgprB4$^+$ neurons.
MrgprA3^{tdTomato}	*MrgprA3$^{Cre-EGFP}$ X ROSA26^{tdTomato}*	to use tdTomato to visualize MrgprA3$^+$ neurons and their peripheral axons.

MrgprC11^{tdTomato}	*MrgprC11^{CreER} X ROSA26^{tdTomato}*	to use tdTomato to visualize MrgprC11^{+} neurons and their peripheral axons.
MrgprD^{tdTomato}	*MrgprD^{CreER} X ROSA26^{tdTomato}*	to use tdTomato to visualize MrgprD^{+} neurons and their peripheral axons.
MrgprC11^{PLAP}	*MrgprC11^{CreER} X ROSA26^{PLAP}*	to use PLAP axonal tracer to visualize MrgprC11^{+} nerves in the airway.
MrgprC11^{DTR}	*MrgprC11^{CreER} X ROSA26^{DTR}*	to specifically ablate MrgprC11^{+} neurons using diphtheria toxin.

Tamoxifen and Diphtheria toxin treatments

To label MrgprC11^{+} neurons and MrgprD^{+} neurons, the *MrgprC11^{CreER}* or *MrgprD^{CreER}* mice were treated daily via oral gavage (22g x 25mm, FTP-22-25, Instech Laboratories) with 100 mg/kg of tamoxifen (T5648, Sigma) dissolved in sunflower seed oil (S5007, Sigma) for 5 days at 3-4 weeks of age. For sparse labeling of MrgprC11^{+} neurons, the mice were treated with low dose of tamoxifen (10mg/kg) once.

6 weeks old *MrgprC11^{CreER} ; ROSA26^{DTR}* mice and *ROSA26^{DTR}* littermates were injected with diphtheria toxin (i.p. 200ng/mouse, Sigma 322326) daily for three consecutive weeks. Airway allergic inflammation models were induced at least four weeks after the first toxin injection.

Ovalbumin-induced airway allergic inflammation

Mice were sensitized to ovalbumin via i.p. injection of 50 µg ovalbumin plus 2mg Imject Alum in 150 µl PBS on days 1, 7, and 14. Lightly anesthetized mice (isoflurane) were challenged by intratracheal instillation of 200 µg ovalbumin in 50 µl PBS on days 21, 22, and 23. Airway mechanics measurements and analysis of the bronchoalveolar lavage fluid (BALF) were performed on day 24. BALF was centrifuged and the cell pellet was resuspended in PBS to perform differential cell counting of leukocytes (macrophages/monocytes, neutrophils, eosinophils, and lymphocytes). The supernatant of BALF was used to examine the levels of IL-4, IL-5, and IFN-γ, using enzyme immunoassay kits (R&D Systems) according to individual kit instructions.

PLAP whole-mount histochemistry staining

The procedure was performed as previously described (36). Briefly, adult mice (8-12 weeks old) were transcardially perfused with ice-cold 4% formaldehyde. Tissues were dissected and postfixed in 4% formaldehyde on ice (30 minutes for DRG and vagal ganglia and 2 hours for the lung) and incubated in HBSS at 65-68 ºC for 30 minutes to inhibit the endogenous alkaline phosphatase. Then tissues were washed with B1 buffer (0.1 M Tris pH 7.5, 0.15 M NaCl), then B3 buffer (0.1 M Tris pH 9.5, 0.1 M NaCl, 50 mM MgCl2), and finally incubated with B3 buffer with 37.5 ug/ml NBT and 175 ug/ml BCIP to visualize the PLAP signals. The tissues were fixed in 4% formaldehyde overnight at 4 ºC and cleared in BABB (Benzyl Alcohol and Benzyl Benzoate, 1:2 mixed together) before imaging on a ZEISS SteREO Discovery V12 stereomicroscope with a color camera.

Immunohistochemistry staining

Immunohistochemistry staining was performed as previously described (29). Briefly, adult mice (8-12 weeks old) were transcardially perfused with fixative (ice-cold 4% formaldehyde and 14% picric acid in PBS). DRGs were dissected, cryoprotected in 30% sucrose, and were sectioned at a thickness of 20 □m. Antibodies used include rabbit anti-MrgprC11 (1:500) which was custom made by Proteintech groups and validated by previous study (6) and donkey anti-Rabbit IgG-Alexa Fluor 555 (Invitrogen, A-31572, 1:500).

RNAscope *in situ* hybridization

RNAscope *in situ* hybridization was performed using the RNAscope® Multiplex Fluorescent Reagent V2 (ACD 323270) according to the manufacturer's instructions. Briefly, vagal ganglia were quickly collected and fresh frozen in dry-ice-cooled OCT medium. The ganglia were

sectioned at a thickness of 20 □m and the following probes were used: Prdmd12 (524371), MrgprA3 (548161), MrgprB4 (435781), MrgprC11 (488771), MrgprD (417921), IL4ra (520171), OSMR (427081), gp130 (476211), TRPV1 (313331). Fluorescent images were acquired on a Confocal Microscopy Zeiss LSM700 and analyzed in Fiji. DAPI staining was performed to visualize the nuclei of the cells. Cells with ≥ 5 fluorescent dots are considered positive. 3000-4000 vagal sensory neurons (3-6 vagal ganglia) were quantified to examine the percentage of neurons expressing each gene. Only cells containing nuclei labeled by DAPI were counted to avoid repetitive counting of the same cells in different sections.

Cell culture and calcium imaging

Vagal sensory neuron culture and calcium imaging were performed as previously described *(69)*. Briefly, Vagal sensory neurons isolated from $Pirt^{GCaMP3/+}$ mice were cultured and used for all calcium imaging analysis. Chemicals used are listed as follows: oncostatin M (300nM, LSBio, LS-G27227), IL-4 (300 nM, bio-techne 404-ML), Bam8-22 (100nM, custom synthesized by Genscript). For every batch of vagal sensory neuron culture, vagal ganglia dissected from 10 $Pirt^{GCaMP3/+}$ mice were pooled together, dissociated, and cultured on coverslips. The cultured cells are a mixture of jugular and nodose neurons as there is no effective way to separate jugular and nodose ganglia during the dissection. A subthreshold concentration of Bam8-22 (100nM) that normally only induces minimal calcium responses in vagal sensory was used to test if IL4 or OSM can sensitize cultured vagal sensory neurons. The same neurons were sequentially challenged with Bam8-22 (100 nM, 30 seconds), followed by IL-4 or OSM or calcium imaging buffer (300 nM, 3 minutes), and then with Bam8-22 (100 nM, 30 seconds) again. Neurons were washed for 60 seconds with calcium imaging buffer after every chemical. After chemical challenges, the number of neurons showing increased GCaMP3 fluorescence intensity and the total cell number are

quantified to calculate the percentage of Bam8-22-responsive vagal sensory neurons. The threshold to identify responsive cells was set as a 20% increase in fluorescence intensity. All calcium imaging experiments were repeated four times with four different batches of cell cultures, with each dot in Figures 4D, 4E, and 5E representing one batch. In each batch, three to four coverslips were tested, with the total cell number ranging from 350-720. On average, 6.25 Bam8-22-responsive neurons were identified during the initial Bam8-22 application, and 22 Bam8-22-responsive neurons were identified after the OSM/IL-4 application in one batch. Fluorescence intensity traces of Bam8-22-responsive neurons from one batch were pooled together to generate the average fluorescence changes trace in Figure 4C and 5F and the population data are presented as mean ± s.e.m.

Vagal ganglia injection

The vagal ganglion was surgically exposed from the ventral side of the neck. Unilateral injections were carried out using custom glass pipettes (pulled by a micropipette puller, Sutter Instruments) that were connected to Eppendorf Femtojet. AAV-EGFP (Addgene viral prep #105542) and Cre-dependent AAV-flex-tdTomato (Addgene vector #51503, virus packaged at Emory Virus Core) were injected directly into the vagal ganglia of *MrgprC11*^{CreER} mice ($1.5\text{-}2.5 \times 10^{12}$ GC/mL, ~0.2 µL for each vagal ganglion). The nodose structure is easily visualized under the dissection microscope after surgical exposure. However, the jugular structure is typically not clearly visible, as it is hidden behind the bones. The AAV virus were injected into the rostral side of the nodose structure and diffused into the jugular. To ensure specific labeling of the jugular neuron, we collected all sensory ganglia including trigeminal ganglia, all cervical and thoracic DRGs and vagal ganglia from the AAV-injected animals. GFP or tdTomato signals in the trigeminal or DRG

ganglia indicate virus leakage and those animals were excluded from the analysis. Only animals showing specific signals in the vagal ganglia were used to collect lung sections.

Airway mechanics

Anesthetized (pentobarbital, 70 mg/kg) animals were tracheotomized, attached to a Flexivent pulmonary mechanics analyzer (SCIREQ), and paralyzed with succinylcholine (2 mg/kg). Anesthetized mice were ventilated at a tidal volume of 9 mL/kg, at a frequency of 150 bpm. Positive end-expiratory pressure was set at 3 cm H_2O. We assessed the airway responsiveness using a single-compartment model to measure the total lung resistance (R_L), a dynamic variable that is largely dependent on the resistance to air flow through the airways and is sensitive to airway smooth muscle contraction. Airway hyperresponsiveness was determined in response to aerosolized methacholine challenges (0, 1, 3, 10, and 30 mg/ml). The nebulizer was on for 10 seconds to deliver each dose of MCh. Bam8-22 (50 µl, 10 mg/ml) were administered by retro-orbital IV injection.

Real-time RT-PCR

Real-time RT-PCR was performed in order to examine the gene expression changes in the VG. Total RNA was extracted from the VG using RNeasy Micro Kits (Qiagen), following the manufacturer's protocol. cDNA was generated using the SuperScript III First-Strand Synthesis System (Invitrogen, Thermo Fisher Scientific, Waltham, MA). Quantitative real-time PCR was performed using a StepOnePlus Real-Time PCR System (Thermo Fisher Scientific) with the SYBR Green detection method. The cycle threshold (C_T) values were analyzed by the $2^{-\Delta CT}$ method to determine the normalized expression ratio of target genes.

The sequence of the primers used were as follows:

MrgprC11-F AGCATCCACAACCCCAGAAG

MrgprC11-R TGGAGTGCAGTTGGGATGAC

Cathepsin S-F CACCACACTTCAGGATGACC

Cathepsin S-R TTCCCAGATGAGACGCCGTA

OSM-F CAGCTGCAGAATCAGGCGAA

OSM-R CTGAGCCCATGAAGCGATGG

OSMR-F GGACTGTCCCAGCCCTTACT

OSMR-R GCACAGCTTCTTCACGCTTC

Statistical Analysis

Data are represented as mean ± SEM. GraphPad Prism scientific software version 9.5.0 was used for statistical analysis. Statistical significance was determined using parametric methods (Welch's t-test, one-way ANOVA, or two-way ANOVA). The specific tests used to analyze each data set is indicated within the individual figure legends. Differences were considered as statistically significant at a value of * $p<0.05$ ** $p<0.01$ ***$p<0.001$ and ***$p<0.0001$.

ACKNOWLEDGMENTS

We thank the Department of Animal Resources at Georgia Institute of Technology for the animal care and services. The work was supported by grants from the US National Institutes of Health (HL141269) and National Science Foundation (2334697) to L.H.

FIGURE LEGEND

Figure 1. Mrgprs are specifically expressed in jugular sensory neurons. (A-D) Expression of Mrgpr family members in both DRGs and VGs using mouse genetic labeling. Mrgprs^{+} DRG sensory neurons are evenly distributed within the ganglia. However, all Mrgprs^{+} vagal sensory neurons are located in the rostral part of the ganglia. Brightfield images were collected for tdTomato labeling to visualize the morphology of the ganglia. (E) RNAscope *in situ* showing that Mrgprs are only expressed in jugular sensory neurons labeled by Prdm12. Arrowheads point to some of the overlapping cells. DAPI-nuclei stain was shown in blue. (F) The expressions of MrgprC11 and MrgprD define two different jugular nociceptive populations. The boxed areas in the upper panels in E&F are shown at greater magnification in the lower panels. (G) Table showing the percentage of jugular neurons expressing Mrgpr family members. Scale bars: A-D, 250 µm, E-F top panel, 100 µm, E-F lower panel, 25 µm.

Figure 2. Whole mount PLAP histochemistry analysis of the airway isolated from *MrgprC11^{PLAP}* mice with tamoxifen treatment to examine the innervation of MrgprC11^{+} nerves. (A-C) *MrgprC11^{PLAP}* mice were treated with high dose of tamoxifen (100mg/kg, once daily for 5 days) to visualize all MrgprC11^{+} nerves. Dense nerves were observed in the larynx (A), trachea (B) and main bronchi (C). The trachea was cut along the anterior midline of the cartilage to make a flat whole-mount. (D-E) *MrgprC11^{PLAP}* mice were treated with low dose of tamoxifen (10mg/kg, once) to sparsely label a subset of MrgprC11^{+} neurons. Terminal arbors were observed in both proximal large airway (D) and distal small airway (E). (F) Lung sections collected from *MrgprC11^{tdTomato}* mice treated with high dose of tamoxifen. MrgprC11^{+} lung interoceptors penetrate into the superficial luminal surface. DAPI-nuclei stain was shown in blue. Scale bars: A-C, 1mm, D-E, 0.1mm, F, 50 µm.

Figure 3. MrgprC11^{+} jugular neurons innervate the lung. (A) Diagram illustrating injection of AAV-EGFP and AAV-flex-tdTomato into the vagal ganglia of *MrgprC11^{CreER}* mice. Created with BioRender.com. (B-D) Light view (B), EGFP (C) and tdTomato (C) images of a injected vagal ganglion. (E) Lung sections of AAV-injected mice showing MrgprC11^{+} nerves in the lung, labeled by both tdTomato and EGFP. Scale bars: B-D, 250 μm, E, 50 μm.

Figure 4. IL-4 in the inflamed airway interacts with jugular neurons and sensitizes MrgprC11^{+} neurons. (A) IL4ra is expressed in both jugular and nodose neurons, although predominantly in jugular neurons. DAPI-nuclei stain was shown in blue. Boxed areas in A are shown at greater magnification in A' and A'' to show IL4ra expression in jugular (A') and nodose (A''). (B) IL4ra^{+} jugular cells exhibit much higher fluorescent intensity of the *in situ* signals compared to IL4ra^{+} nodose neurons. Average fluorescence intensity were collected from 250 IL4ra^{+} jugular neurons and 62 IL4ra^{+} nodose neurons in 4 vagal ganglia isolated from 3 mice. (C) The majority of MrgprC11^{+} neurons express IL4ra. Venn Diagrams on the right illustrating the relative expression pattern and the numbers in the diagram indicate the cell numbers quantified. The sizes of the circles are proportional to the sizes of the cell populations. (D) Calcium responses of Bam8-22-sensitive neurons (100 nM Bam8-22) before and after IL-4 treatment (300 nM, 3 min). Average fluorescence changes (ΔF/F) were calculated from ≥ 20 cells and the population data are presented as mean ± s.e.m. (E) IL-4 increased the percentage of Bam8-22-responsive vagal sensory neurons. (F) The percentage of Bam8-22-responsive vagal sensory neurons did not change when neurons were incubated with calcium imaging buffer between the two Bam8-22 applications. Welch's t-test for E. *$p < 0.05$. Scale bars: A, 100 μm, A', A'', and C, 25 μm.

Figure 5. Oncostatin M in the inflamed airway interacts with jugular neurons and sensitizes MrgprC11^{+} neurons. (A-B) Oncostatin M receptor subunits OSMR and gp130 are mainly

expressed in jugular neurons. The boxed areas in A are shown at greater magnification in B. (C) More than half of the MrgprC11$^+$ neurons express OSMR. Venn Diagrams on the right illustrating the relative expression pattern and the numbers in the diagram indicate the cell numbers quantified. The sizes of the circles are proportional to the sizes of the cell populations. DAPI-nuclei stain was shown in blue in A-C. (D) OSM expression is upregulated in the inflamed lung. (E) OSM increased the percentage of Bam8-22-responsive vagal sensory neurons. (F) Calcium responses of Bam8-22-sensitive neurons (100 nM Bam8-22) before and after OSM treatment (300 nM, 3 min). Average fluorescence changes ($\Delta F/F$) were calculated from ≥ 20 cells and the population data are presented as mean ± s.e.m. Welch's t-test for D-E. *$p < 0.05$. Scale bars: A, 100 µm, B-C, 25 µm.

Figure 6. Allergic airway inflammation sensitizes MrgprC11$^+$ jugular neurons. (A-B) RNAscope *in situ* showing the increased percentage of MrgprC11$^+$ neurons in jugular neurons in asthmatic mice. Representative images of vagal ganglia sections from naïve and OVA-treated mice are shown in (A). The boxed areas in the upper panels are shown at greater magnification in the lower panels. The average percentages of MrgprC11$^+$ neurons in jugular ganglia are shown in B. DAPI-nuclei stain was shown in blue in A. (C) Real time PCR analysis showing increased MrgprC11 mRNA level in vagal ganglia in inflamed mice. (D) Bam8-22-induced bronchoconstriction was also significantly increased in the inflamed mice. (E) Real time PCR analysis showing increased cathepsin S expression level in the inflamed lung. Welch's t-test for B, C, and E. Two-way ANOVA for D. *$p < 0.05$, **$p < 0.01$, ****$p < 0.0001$. Scale bars: A top panel , 100 µm, lower panel, 25 µm.

Figure 7. Ablation of MrgprC11$^+$ jugular neurons blocked AHR. (A-B) MrgprC11$^+$ neurons were ablated in DTX-treated *MrgprC11^{DTR}* mice. Scale bars 50 µm. (C-F) Ablation of MrgprC11$^+$ neurons did not affect the inflammatory cell count in BALF (C) and the level of IL-4 (D), IL-5

(E), and IFNɣ (F). (G) Ablation of MrgprC11^{+} neurons blocked airway hyperresponsiveness. Data collected for the 30 mg/ml MCh was replotted in dot plot in (H) to better visualize the differences between the control and cell ablation groups. Two-way ANOVA *p < 0.05, **p < 0.01. Scale bars: A, 100 µm.

SUPPLEMENTAL FIGURE LEGEND

Figure S1. Expression of OSMR in jugular ganglia in naïve and OVA-treated mice. (A) RNAscope *in situ* showing the expression of OSMR and Prdm12 in naïve and asthmatic mice. The boxed areas in the upper panels are shown at greater magnification in the lower panels. DAPI-nuclei stain was shown in blue. (B) The percentages of OSMR^{+} neurons in jugular are comparable in naïve mice and asthmatic mice. (C) qPCR analysis of vagal ganglia showing that OSMR expression is decreased in the vagal sensory neurons in the inflamed mice. Scale bars: A top panel , 100 µm, lower panel, 25 µm.

Figure S2. Expression of IL4ra in naïve and OVA-treated mice. (A) RNAscope *in situ* showing the expression of IL4ra and Prdm12 in vagal ganglia from naïve and asthmatic mice. The boxed areas in the upper panels are shown at greater magnification in the lower panels. DAPI-nuclei stain was shown in blue. (B) The percentages of IL4ra^{+} neurons in the jugular ganglia are comparable in naïve mice and asthmatic mice. (C) The percentages of IL4ra^{+} neurons in the vagal ganglia are comparable in naïve mice and asthmatic mice. (D) qPCR analysis of vagal ganglia showing comparable expression of IL4ra in naïve and inflamed mice. Welch's t-test. Scale bars: A top panel , 100 µm, lower panel, 25 µm.

Figure S3. Expression of TRPV1 and MrgprC11 in naïve and OVA-treated mice. (A) RNAscope *in situ* showing the expression of TRPV1 and MrgprC11 in vagal ganglia from naïve and asthmatic mice. The boxed areas in the upper panels are shown at greater magnification in the lower panels. DAPI-nuclei stain was shown in blue. (B) The percentages of $TRPV1^{+}$ neurons expressing MrgprC11 is increased in OVA-treated mice. (C) The percentages of $MrgprC11^{+}$ neurons expressing TRPV1 are comparable in naïve mice and asthmatic mice. Welch's t-test for B. *$p < 0.05$. Scale bars: A top panel , 100 µm, lower panel, 25 µm.

REFERENCES

1. Barnes PJ. Overview of neural mechanisms in asthma. Pulm Pharmacol. 1995;8:151-159.
2. Undem BJ, Carr MJ. The role of nerves in asthma. Curr Allergy Asthma Rep. 2002;2:159-165.
3. Trevor JL, Deshane JS. Refractory asthma: mechanisms, targets, and therapy. Allergy. 2014;69:817-827.
4. Masato Tamari KLDB, Aaron M. Ver Heul, Lydia Zamidar, Keisuke Orimo, Masato Hoshi, Anna M. Trier, Ting-Lin Yang, Catherine M. Biggs, Gargi Damle, Deniz Demircioglu, Dan Hasson, Jinye Dai, Hideaki Morita, Kenji Matsumoto, Sanjay Jain, Steven Van Dyken, Joshua D. Milner, Dusan Bogunovic,Hongzhen Hu, David Artis, Stuart E. Turvey, Brian S. Kim. Sensory Neurons Promote Immune Homeostasis in the Lung. Cell Sneak Peak. 2023.
5. Talbot S, Doyle B, Huang J, Wang JC, Ahmadi M, Roberson DP, Yekkirala A, Foster SL, Browne LE, Bean BP, Levy BD, Woolf CJ. Vagal sensory neurons drive mucous cell metaplasia. J Allergy Clin Immunol. 2020;145:1693-1696 e1694.
6. Han L, Limjunyawong N, Ru F, Li Z, Hall OJ, Steele H, Zhu Y, Wilson J, Mitzner W, Kollarik M, Undem BJ, Canning BJ, Dong X. Mrgprs on vagal sensory neurons contribute to bronchoconstriction and airway hyper-responsiveness. Nat Neurosci. 2018;21:324-328.
7. Baral P, Umans BD, Li L, Wallrapp A, Bist M, Kirschbaum T, Wei Y, Zhou Y, Kuchroo VK, Burkett PR, Yipp BG, Liberles SD, Chiu IM. Nociceptor sensory neurons suppress neutrophil and gammadelta T cell responses in bacterial lung infections and lethal pneumonia. Nat Med. 2018;24:417-426.
8. Wallrapp A, Riesenfeld SJ, Burkett PR, Abdulnour RE, Nyman J, Dionne D, Hofree M, Cuoco MS, Rodman C, Farouq D, Haas BJ, Tickle TL, Trombetta JJ, Baral P, Klose CSN, Mahlakoiv T, Artis D, Rozenblatt-Rosen O, Chiu IM, Levy BD, Kowalczyk MS, Regev A, Kuchroo VK. The neuropeptide NMU amplifies ILC2-driven allergic lung inflammation. Nature. 2017;549:351-356.
9. Talbot S, Abdulnour RE, Burkett PR, Lee S, Cronin SJ, Pascal MA, Laedermann C, Foster SL, Tran JV, Lai N, Chiu IM, Ghasemlou N, DiBiase M, Roberson D, Von Hehn C, Agac B, Haworth O, Seki H, Penninger JM, Kuchroo VK, Bean BP, Levy BD, Woolf CJ. Silencing Nociceptor Neurons Reduces Allergic Airway Inflammation. Neuron. 2015;87:341-354.
10. Su Y, Barr J, Jaquish A, Xu J, Verheyden JM, Sun X. Identification of lung innervating sensory neurons and their target specificity. Am J Physiol Lung Cell Mol Physiol. 2022;322:L50-L63.
11. Crosson T, Wang JC, Doyle B, Merrison H, Balood M, Parrin A, Pascal M, Mindt BC, Seehus CR, Ozcan A, Huang X, Semenara E, Lai NYY, Majdoubi A, Abdulnour RE, Rajchgot T, Rafei M, Foster SL, Thibodeau J, Fritz JH, Levy BD, Woolf CJ, Talbot S. FcepsilonR1-expressing nociceptors trigger allergic airway inflammation. J Allergy Clin Immunol. 2021;147:2330-2342.
12. Trankner D, Hahne N, Sugino K, Hoon MA, Zuker C. Population of sensory neurons essential for asthmatic hyperreactivity of inflamed airways. Proc Natl Acad Sci U S A. 2014;111:11515-11520.
13. Caceres AI, Brackmann M, Elia MD, Bessac BF, del Camino D, D'Amours M, Witek JS, Fanger CM, Chong JA, Hayward NJ, Homer RJ, Cohn L, Huang X, Moran MM, Jordt SE. A sensory neuronal ion channel essential for airway inflammation and hyperreactivity in asthma. Proc Natl Acad Sci U S A. 2009;106:9099-9104.
14. McAlexander MA, Gavett SH, Kollarik M, Undem BJ. Vagotomy reverses established allergen-induced airway hyperreactivity to methacholine in the mouse. Respir Physiol Neurobiol. 2015;212-214:20-24.
15. Mazzone SB, Canning BJ. Autonomic neural control of the airways. Handb Clin Neurol. 2013;117:215-228.
16. Taylor-Clark TE, Undem BJ. Neural control of the lower airways: Role in cough and airway inflammatory disease. Handb Clin Neurol. 2022;188:373-391.
17. Mazzone SB, Undem BJ. Vagal Afferent Innervation of the Airways in Health and Disease. Physiol Rev. 2016;96:975-1024.
18. Wang J, Kollarik M, Ru F, Sun H, McNeil B, Dong X, Stephens G, Korolevich S, Brohawn P, Kolbeck R, Undem B. Distinct and common expression of receptors for inflammatory mediators in vagal nodose

versus jugular capsaicin-sensitive/TRPV1-positive neurons detected by low input RNA sequencing. PLoS One. 2017;12:e0185985.
19. Klein Wolterink RGJ, Wu GS, Chiu IM, Veiga-Fernandes H. Neuroimmune Interactions in Peripheral Organs. Annual review of neuroscience. 2022;45:339-360.
20. Canning BJ, Spina D. Sensory nerves and airway irritability. Handb Exp Pharmacol. 2009;194:139-183.
21. Barnes PJ. Neuroeffector mechanisms: the interface between inflammation and neuronal responses. J Allergy Clin Immunol. 1996;98:S73-81; discussion S81-73.
22. Myers AC, Kajekar R, Undem BJ. Allergic inflammation-induced neuropeptide production in rapidly adapting afferent nerves in guinea pig airways. Am J Physiol Lung Cell Mol Physiol. 2002;282:L775-781.
23. Wallrapp A, Burkett PR, Riesenfeld SJ, Kim SJ, Christian E, Abdulnour RE, Thakore PI, Schnell A, Lambden C, Herbst RH, Khan P, Tsujikawa K, Xavier RJ, Chiu IM, Levy BD, Regev A, Kuchroo VK. Calcitonin Gene-Related Peptide Negatively Regulates Alarmin-Driven Type 2 Innate Lymphoid Cell Responses. Immunity. 2019;51:709-723 e706.
24. Chapman DG, Irvin CG. Mechanisms of airway hyper-responsiveness in asthma: the past, present and yet to come. Clin Exp Allergy. 2015;45:706-719.
25. Su Y, Xu J, Zhu Z, Chin J, Xu L, Yu H, Nudell V, Dash B, Moya EA, Ye L, Nimmerjahn A, Sun X. Brainstem Dbh(+) neurons control allergen-induced airway hyperreactivity. Nature. 2024;631:601-609.
26. Liu Q, Dong X. The role of the Mrgpr receptor family in itch. Handb Exp Pharmacol. 2015;226:71-88.
27. Zhu Y, Hanson CE, Liu Q, Han L. Mrgprs activation is required for chronic itch conditions in mice. Itch (Phila). 2017;2.
28. Han L, Ma C, Liu Q, Weng HJ, Cui Y, Tang Z, Kim Y, Nie H, Qu L, Patel KN, Li Z, McNeil B, He S, Guan Y, Xiao B, Lamotte RH, Dong X. A subpopulation of nociceptors specifically linked to itch. Nat Neurosci. 2013;16:174-182.
29. Steele HR, Xing Y, Zhu Y, Hilley HB, Lawson K, Nho Y, Niehoff T, Han L. MrgprC11(+) sensory neurons mediate glabrous skin itch. Proc Natl Acad Sci U S A. 2021;118.
30. Liu Q, Vrontou S, Rice FL, Zylka MJ, Dong X, Anderson DJ. Molecular genetic visualization of a rare subset of unmyelinated sensory neurons that may detect gentle touch. Nat Neurosci. 2007;10:946-948.
31. Vrontou S, Wong AM, Rau KK, Koerber HR, Anderson DJ. Genetic identification of C fibres that detect massage-like stroking of hairy skin in vivo. Nature. 2013;493:669-673.
32. Elias LJ, Succi IK, Schaffler MD, Foster W, Gradwell MA, Bohic M, Fushiki A, Upadhyay A, Ejoh LL, Schwark R, Frazer R, Bistis B, Burke JE, Saltz V, Boyce JE, Jhumka A, Costa RM, Abraira VE, Abdus-Saboor I. Touch neurons underlying dopaminergic pleasurable touch and sexual receptivity. Cell. 2023;186:577-590 e516.
33. Cavanaugh DJ, Lee H, Lo L, Shields SD, Zylka MJ, Basbaum AI, Anderson DJ. Distinct subsets of unmyelinated primary sensory fibers mediate behavioral responses to noxious thermal and mechanical stimuli. Proc Natl Acad Sci U S A. 2009;106:9075-9080.
34. Liu Q, Sikand P, Ma C, Tang Z, Han L, Li Z, Sun S, LaMotte RH, Dong X. Mechanisms of itch evoked by beta-alanine. J Neurosci. 2012;32:14532-14537.
35. Abdus-Saboor I, Fried NT, Lay M, Burdge J, Swanson K, Fischer R, Jones J, Dong P, Cai W, Guo X, Tao YX, Bethea J, Ma M, Dong X, Ding L, Luo W. Development of a Mouse Pain Scale Using Sub-second Behavioral Mapping and Statistical Modeling. Cell Rep. 2019;28:1623-1634 e1624.
36. Xing Y, Steele HR, Hilley HB, Zhu Y, Lawson K, Niehoff T, Han L. Visualizing the Itch-Sensing Skin Arbors. The Journal of investigative dermatology. 2021;141:1308-1316.
37. Dong X, Han S, Zylka MJ, Simon MI, Anderson DJ. A diverse family of GPCRs expressed in specific subsets of nociceptive sensory neurons. Cell. 2001;106:619-632.
38. Liu Q, Tang Z, Surdenikova L, Kim S, Patel KN, Kim A, Ru F, Guan Y, Weng HJ, Geng Y, Undem BJ, Kollarik M, Chen ZF, Anderson DJ, Dong X. Sensory neuron-specific GPCR Mrgprs are itch receptors mediating chloroquine-induced pruritus. Cell. 2009;139:1353-1365.
39. Badea TC, Hua ZL, Smallwood PM, Williams J, Rotolo T, Ye X, Nathans J. New mouse lines for the analysis of neuronal morphology using CreER(T)/loxP-directed sparse labeling. PLoS One. 2009;4:e7859.

40. Wu H, Williams J, Nathans J. Morphologic diversity of cutaneous sensory afferents revealed by genetically directed sparse labeling. eLife. 2012;1:e00181.
41. Xing Y, Nho Y, Lawson K, Steele H, Han L. Regional Differences in Itch Transmission. The Journal of investigative dermatology. 2024.
42. Kim SH, Patil MJ, Hadley SH, Bahia PK, Butler SG, Madaram M, Taylor-Clark TE. Mapping of the Sensory Innervation of the Mouse Lung by Specific Vagal and Dorsal Root Ganglion Neuronal Subsets. eNeuro. 2022;9.
43. Kupari J, Haring M, Agirre E, Castelo-Branco G, Ernfors P. An Atlas of Vagal Sensory Neurons and Their Molecular Specialization. Cell Rep. 2019;27:2508-2523 e2504.
44. Liu Y, Diaz de Arce, A., Krasnow, MA. Molecular, anatomical, and functional organization of lung interoceptors. BioRxiv. 2021.
45. Prescott SL, Umans BD, Williams EK, Brust RD, Liberles SD. An Airway Protection Program Revealed by Sweeping Genetic Control of Vagal Afferents. Cell. 2020;181:574-589 e514.
46. Bai L, Mesgarzadeh S, Ramesh KS, Huey EL, Liu Y, Gray LA, Aitken TJ, Chen Y, Beutler LR, Ahn JS, Madisen L, Zeng H, Krasnow MA, Knight ZA. Genetic Identification of Vagal Sensory Neurons That Control Feeding. Cell. 2019;179:1129-1143 e1123.
47. Oetjen LK, Mack MR, Feng J, Whelan TM, Niu H, Guo CJ, Chen S, Trier AM, Xu AZ, Tripathi SV, Luo J, Gao X, Yang L, Hamilton SL, Wang PL, Brestoff JR, Council ML, Brasington R, Schaffer A, Brombacher F, Hsieh CS, Gereau RWt, Miller MJ, Chen ZF, Hu H, Davidson S, Liu Q, Kim BS. Sensory Neurons Co-opt Classical Immune Signaling Pathways to Mediate Chronic Itch. Cell. 2017;171:217-228 e213.
48. Kim YS, Chu Y, Han L, Li M, Li Z, Lavinka PC, Sun S, Tang Z, Park K, Caterina MJ, Ren K, Dubner R, Wei F, Dong X. Central terminal sensitization of TRPV1 by descending serotonergic facilitation modulates chronic pain. Neuron. 2014;81:873-887.
49. Pothoven KL, Norton JE, Suh LA, Carter RG, Harris KE, Biyasheva A, Welch K, Shintani-Smith S, Conley DB, Liu MC, Kato A, Avila PC, Hamid Q, Grammer LC, 3rd, Peters AT, Kern RC, Tan BK, Schleimer RP. Neutrophils are a major source of the epithelial barrier disrupting cytokine oncostatin M in patients with mucosal airways disease. J Allergy Clin Immunol. 2017;139:1966-1978 e1969.
50. Kang HJ, Kang JS, Lee SH, Hwang SJ, Chae SW, Woo JS, Lee HM. Upregulation of oncostatin m in allergic rhinitis. Laryngoscope. 2005;115:2213-2216.
51. Simpson JL, Baines KJ, Boyle MJ, Scott RJ, Gibson PG. Oncostatin M (OSM) is increased in asthma with incompletely reversible airflow obstruction. Exp Lung Res. 2009;35:781-794.
52. Miller M, Beppu A, Rosenthal P, Pham A, Das S, Karta M, Song DJ, Vuong C, Doherty T, Croft M, Zuraw B, Zhang X, Gao X, Aceves S, Chouiali F, Hamid Q, Broide DH. Fstl1 Promotes Asthmatic Airway Remodeling by Inducing Oncostatin M. J Immunol. 2015;195:3546-3556.
53. Headland SE, Dengler HS, Xu D, Teng G, Everett C, Ratsimandresey RA, Yan D, Kang J, Ganeshan K, Nazarova EV, Gierke S, Wedeles CJ, Guidi R, DePianto DJ, Morshead KB, Huynh A, Mills J, Flanagan S, Hambro S, Nunez V, Klementowicz JE, Shi Y, Wang J, Bevers J, 3rd, Ramirez-Carrozzi V, Pappu R, Abbas A, Vander Heiden J, Choy DF, Yadav R, Modrusan Z, Panettieri RA, Jr., Koziol-White C, Jester WF, Jr., Jenkins BJ, Cao Y, Clarke C, Austin C, Lafkas D, Xu M, Wolters PJ, Arron JR, West NR, Wilson MS. Oncostatin M expression induced by bacterial triggers drives airway inflammatory and mucus secretion in severe asthma. Sci Transl Med. 2022;14:eabf8188.
54. Tseng PY, Hoon MA. Oncostatin M can sensitize sensory neurons in inflammatory pruritus. Sci Transl Med. 2021;13:eabe3037.
55. Jones SA, Jenkins BJ. Recent insights into targeting the IL-6 cytokine family in inflammatory diseases and cancer. Nat Rev Immunol. 2018;18:773-789.
56. Fajardo I, Svensson L, Bucht A, Pejler G. Increased levels of hypoxia-sensitive proteins in allergic airway inflammation. Am J Respir Crit Care Med. 2004;170:477-484.
57. Lewis CC, Yang JY, Huang X, Banerjee SK, Blackburn MR, Baluk P, McDonald DM, Blackwell TS, Nagabhushanam V, Peters W, Voehringer D, Erle DJ. Disease-specific gene expression profiling in multiple models of lung disease. Am J Respir Crit Care Med. 2008;177:376-387.

58. Mathur S, Wang JC, Seehus CR, Poirier F, Crosson T, Hsieh YC, Doyle B, Lee S, Woolf CJ, Foster SL, Talbot S. Nociceptor neurons promote IgE class switch in B cells. JCI Insight. 2021;6.
59. Prescott SL, Liberles SD. Internal senses of the vagus nerve. Neuron. 2022;110:579-599.
60. McGovern AE, Driessen AK, Simmons DG, Powell J, Davis-Poynter N, Farrell MJ, Mazzone SB. Distinct brainstem and forebrain circuits receiving tracheal sensory neuron inputs revealed using a novel conditional anterograde transsynaptic viral tracing system. J Neurosci. 2015;35:7041-7055.
61. Driessen AK, Farrell MJ, Dutschmann M, Stanic D, McGovern AE, Mazzone SB. Reflex regulation of breathing by the paratrigeminal nucleus via multiple bulbar circuits. Brain Struct Funct. 2018;223:4005-4022.
62. Driessen AK, Farrell MJ, Mazzone SB, McGovern AE. The Role of the Paratrigeminal Nucleus in Vagal Afferent Evoked Respiratory Reflexes: A Neuroanatomical and Functional Study in Guinea Pigs. Front Physiol. 2015;6:378.
63. Moe AAK, Bautista TG, Trewella MW, Korim WS, Yao ST, Behrens R, Driessen AK, McGovern AE, Mazzone SB. Investigation of vagal sensory neurons in mice using optical vagal stimulation and tracheal neuroanatomy. iScience. 2024;27:109182.
64. Locksley RM. Asthma and allergic inflammation. Cell. 2010;140:777-783.
65. Kim HY, DeKruyff RH, Umetsu DT. The many paths to asthma: phenotype shaped by innate and adaptive immunity. Nat Immunol. 2010;11:577-584.
66. West NR, Owens BMJ, Hegazy AN. The oncostatin M-stromal cell axis in health and disease. Scand J Immunol. 2018;88:e12694.
67. Behrens R, McGovern AE, Farrell MJ, Moe AAK, Mazzone SB. Mini Review: Central Organization of Airway Afferent Nerve Circuits. Neurosci Lett. 2021;744:135604.
68. Olson W, Abdus-Saboor I, Cui L, Burdge J, Raabe T, Ma M, Luo W. Sparse genetic tracing reveals regionally specific functional organization of mammalian nociceptors. eLife. 2017;6.
69. Nho Y, Lawson K, Banovic F, Han L. Staphylococcus aureus phenol-soluble modulins induce itch sensation. J Dermatol Sci. 2022;107:48-51.

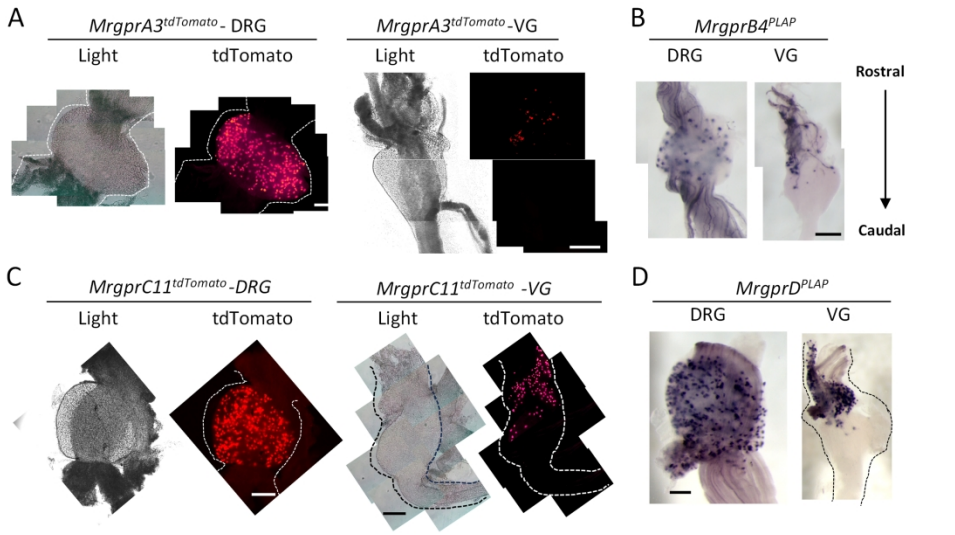

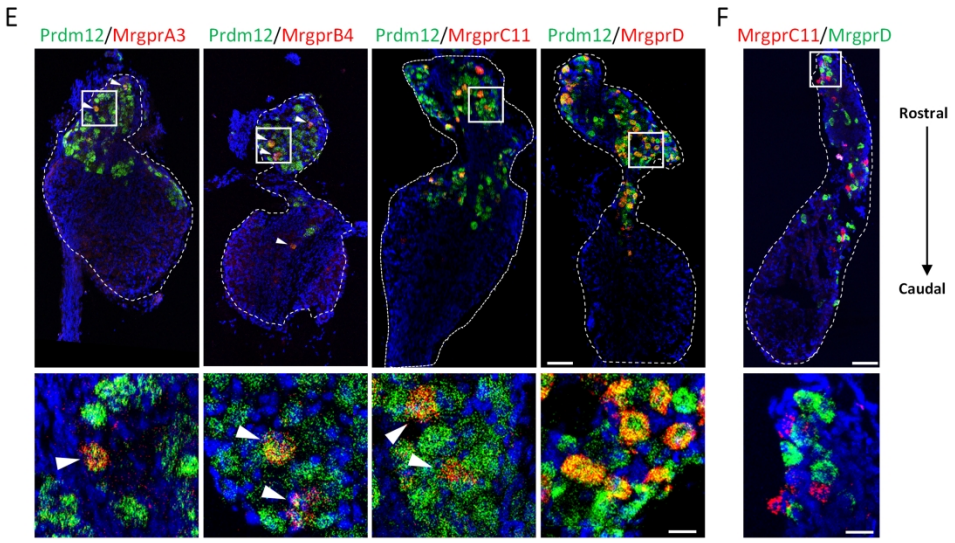

G

	MrgprA3	MrgprB4	MrgprC11	MrgprD
% in jugular neurons (Prdm12+)	1.32%	3.61%	20.31%	37.30%

Figure 1. Mrgprs are specifically expressed in jugular sensory neurons. (A-D) Expression of Mrgpr family members in both DRGs and VGs using mouse genetic labeling. Mrgprs+ DRG sensory neurons are evenly distributed within the ganglia. However, all Mrgprs+ vagal sensory neurons are located in the rostral part of the ganglia. Brightfield images were collected for tdTomato labeling to visualize the morphology of the ganglia. (E) RNAscope in situ showing that Mrgprs are only expressed in jugular sensory neurons labeled by Prdm12. Arrowheads point to some of the overlapping cells. DAPI-nuclei stain was shown in blue. (F) The expressions of MrgprC11 and MrgprD define two different jugular nociceptive populations. The boxed areas in the upper panels in E&F are shown at greater magnification in the lower panels. (G) Table showing the percentage of jugular neurons expressing Mrgpr family members. Scale bars: A-D, 250 μm, E-F top panel, 100 μm, E-F lower panel, 25 μm.

335x419mm (300 x 300 DPI)

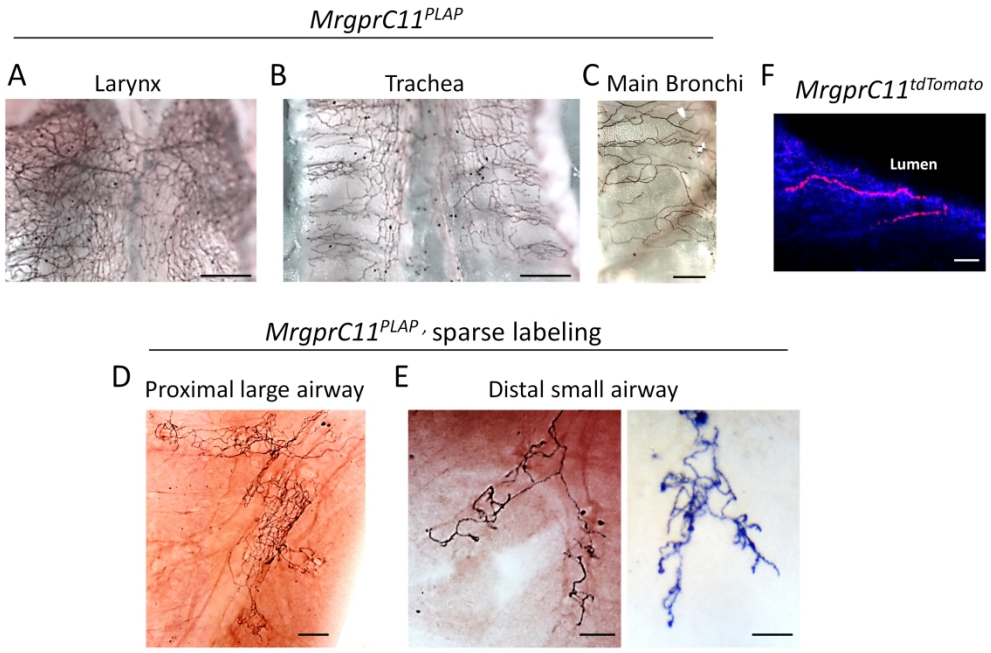

Figure 2. Whole mount PLAP histochemistry analysis of the airway isolated from MrgprC11PLAP mice with tamoxifen treatment to examine the innervation of MrgprC11+ nerves. (A-C) MrgprC11PLAP mice were treated with high dose of tamoxifen (100mg/kg, once daily for 5 days) to visualize all MrgprC11+ nerves. Dense nerves were observed in the larynx (A), trachea (B) and main bronchi (C). The trachea was cut along the anterior midline of the cartilage to make a flat whole-mount. (D-E) MrgprC11PLAP mice were treated with low dose of tamoxifen (10mg/kg, once) to sparsely label a subset of MrgprC11+ neurons. Terminal arbors were observed in both proximal large airway (D) and distal small airway (E). (F) Lung sections collected from MrgprC11tdTomato mice treated with high dose of tamoxifen. MrgprC11+ lung interoceptors penetrate into the superficial luminal surface. DAPI-nuclei stain was shown in blue. Scale bars: A-C, 1mm, D-E, 0.1mm, F, 50 μm.

443x297mm (300 x 300 DPI)

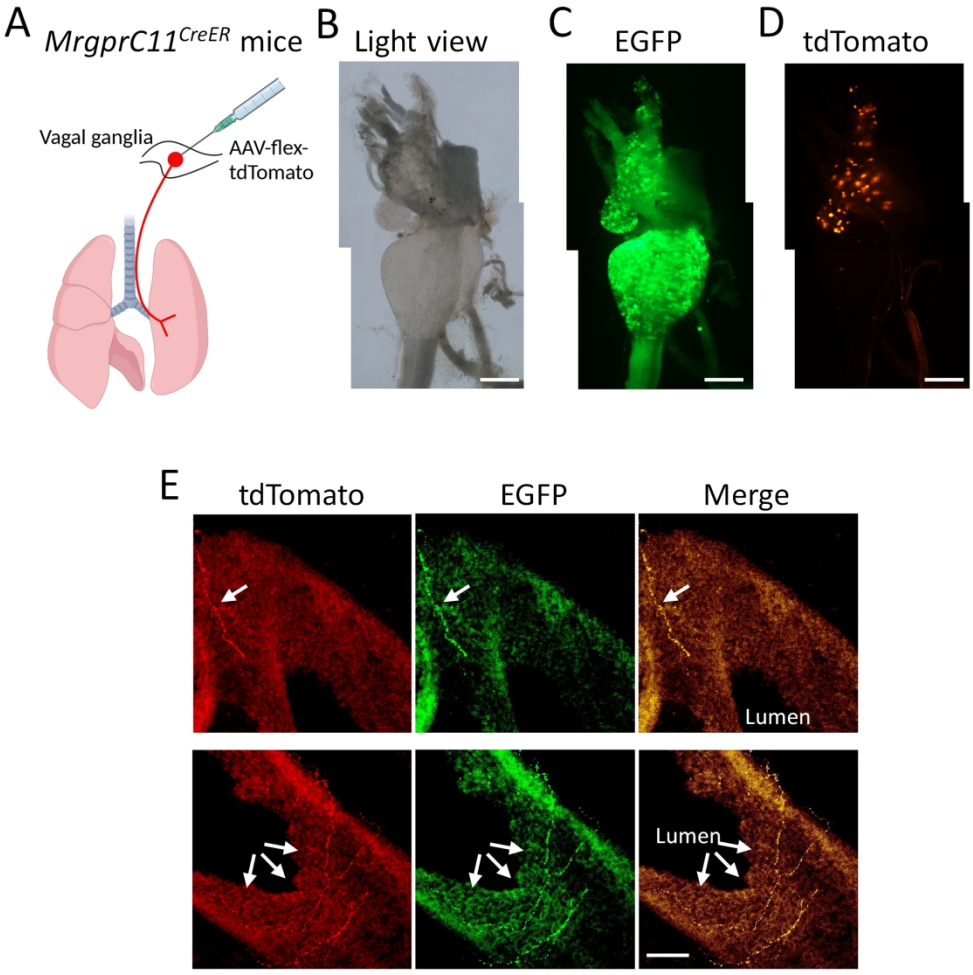

Figure 3. MrgprC11+ jugular neurons innervate the lung. (A) Diagram illustrating injection of AAV-EGFP and AAV-flex-tdTomato into the vagal ganglia of MrgprC11CreER mice. (B-D) Light view (B), EGFP (C) and tdTomato (C) images of a injected vagal ganglion. (E) Lung sections of AAV-injected mice showing MrgprC11+ nerves in the lung, labeled by both tdTomato and EGFP. Scale bars: B-D, 250 μm, E, 50 μm.

339x333mm (300 x 300 DPI)

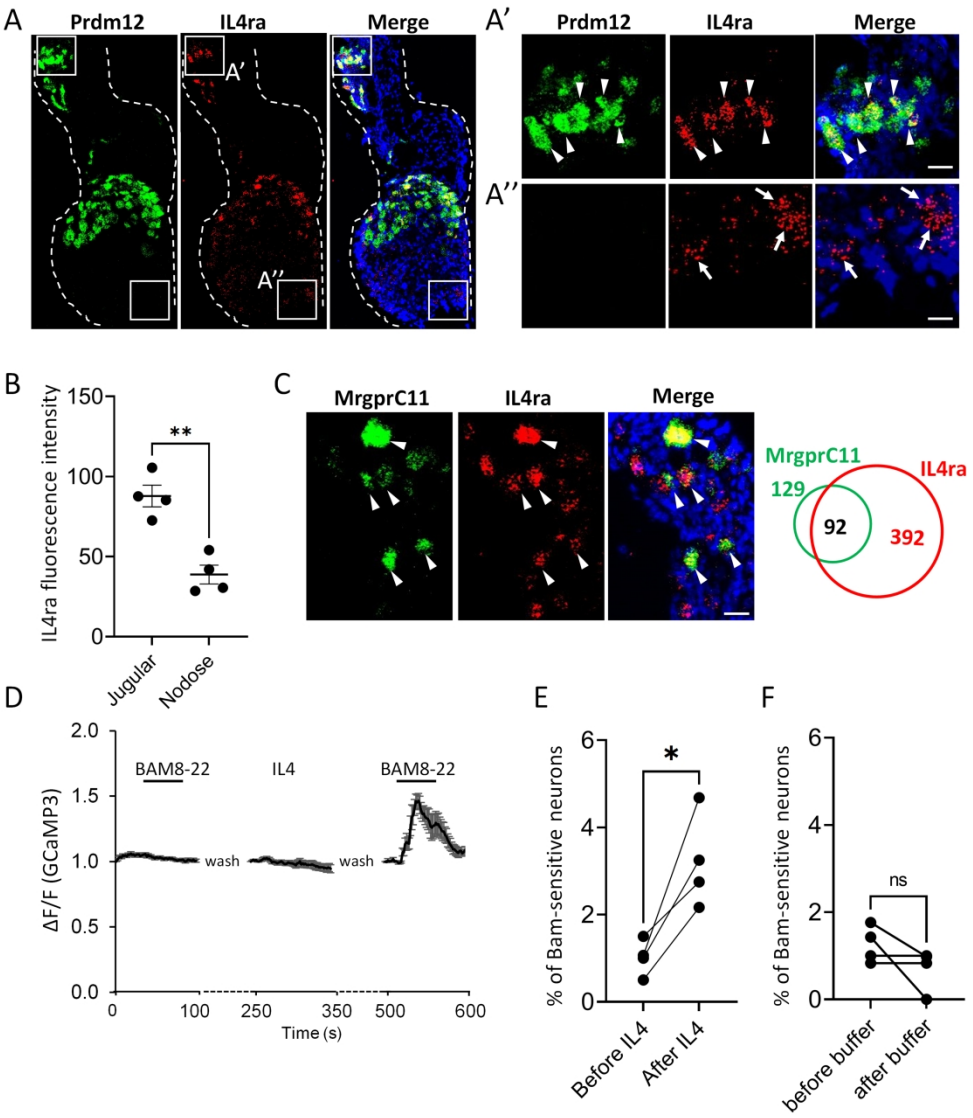

Figure 4. IL-4 in the inflamed airway interacts with jugular neurons and sensitizes MrgprC11+ neurons. (A) IL4ra is expressed in both jugular and nodose neurons, although predominantly in jugular neurons. DAPI-nuclei stain was shown in blue. Boxed areas in A are shown at greater magnification in A' and A'' to show IL4ra expression in jugular (A') and nodose (A''). (B) IL4ra+ jugular cells exhibit much higher fluorescent intensity of the in situ signals compared to IL4ra+ nodose neurons. Average fluorescence intensity were collected from 250 IL4ra+ jugular neurons and 62 IL4ra+ nodose neurons in 4 vagal ganglia isolated from 3 mice. (C) The majority of MrgprC11+ neurons express IL4ra. Venn Diagrams on the right illustrating the relative expression pattern and the numbers in the diagram indicate the cell numbers quantified. The sizes of the circles are proportional to the sizes of the cell populations. (D) Calcium responses of Bam8-22-sensitive neurons (100 nM Bam8-22) before and after IL-4 treatment (300 nM, 3 min). Average fluorescence changes (ΔF/F) were calculated from ≥ 20 cells and the population data are presented as mean ± s.e.m. (E) IL-4 increased the percentage of Bam8-22-responsive vagal sensory neurons. (F) The percentage of Bam8-22-responsive vagal sensory neurons did not change when neurons were incubated with calcium imaging buffer between the two Bam8-22 applications. Welch's t-test for E. *p < 0.05. Scale bars: A, 100 μm, A', A'', and C, 25 μm.

391x436mm (300 x 300 DPI)

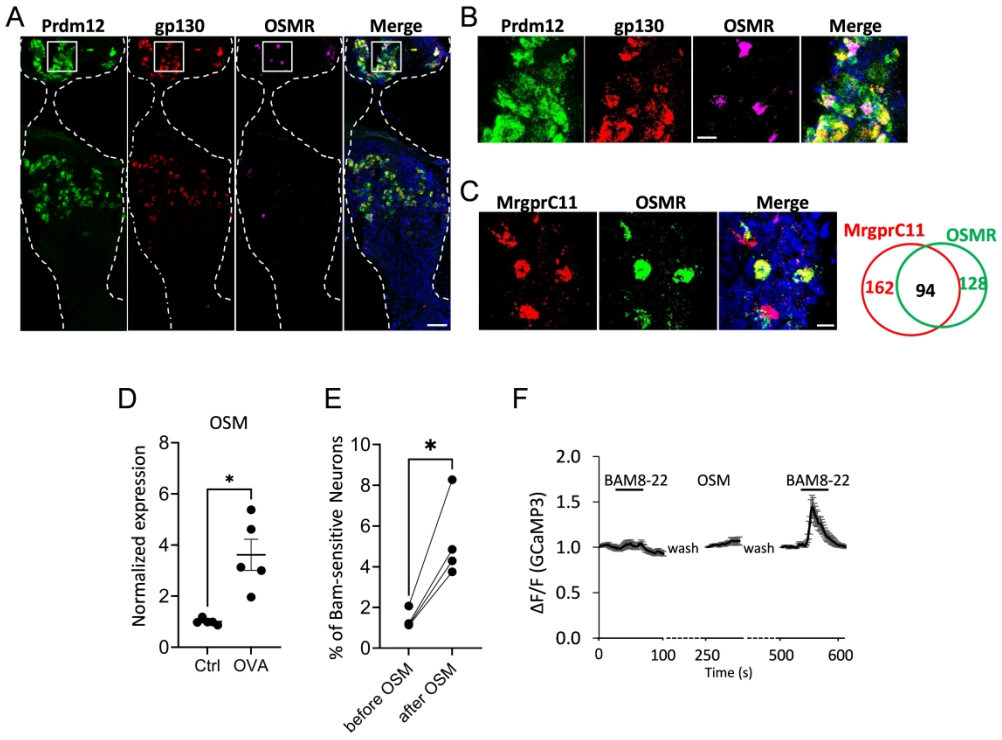

Figure 5. Oncostatin M in the inflamed airway interacts with jugular neurons and sensitizes MrgprC11+ neurons. (A-B) Oncostatin M receptor subunits OSMR and gp130 are mainly expressed in jugular neurons. The boxed areas in A are shown at greater magnification in B. (C) More than half of the MrgprC11+ neurons express OSMR. Venn Diagrams on the right illustrating the relative expression pattern and the numbers in the diagram indicate the cell numbers quantified. The sizes of the circles are proportional to the sizes of the cell populations. DAPI-nuclei stain was shown in blue in A-C. (D) OSM expression is upregulated in the inflamed lung. (E) OSM increased the percentage of Bam8-22-responsive vagal sensory neurons. (F) Calcium responses of Bam8-22-sensitive neurons (100 nM Bam8-22) before and after OSM treatment (300 nM, 3 min). Average fluorescence changes (ΔF/F) were calculated from ≥ 20 cells and the population data are presented as mean ± s.e.m. Welch's t-test for D-E. *p < 0.05. Scale bars: A, 100 μm, B-C, 25 μm.

432x321mm (300 x 300 DPI)

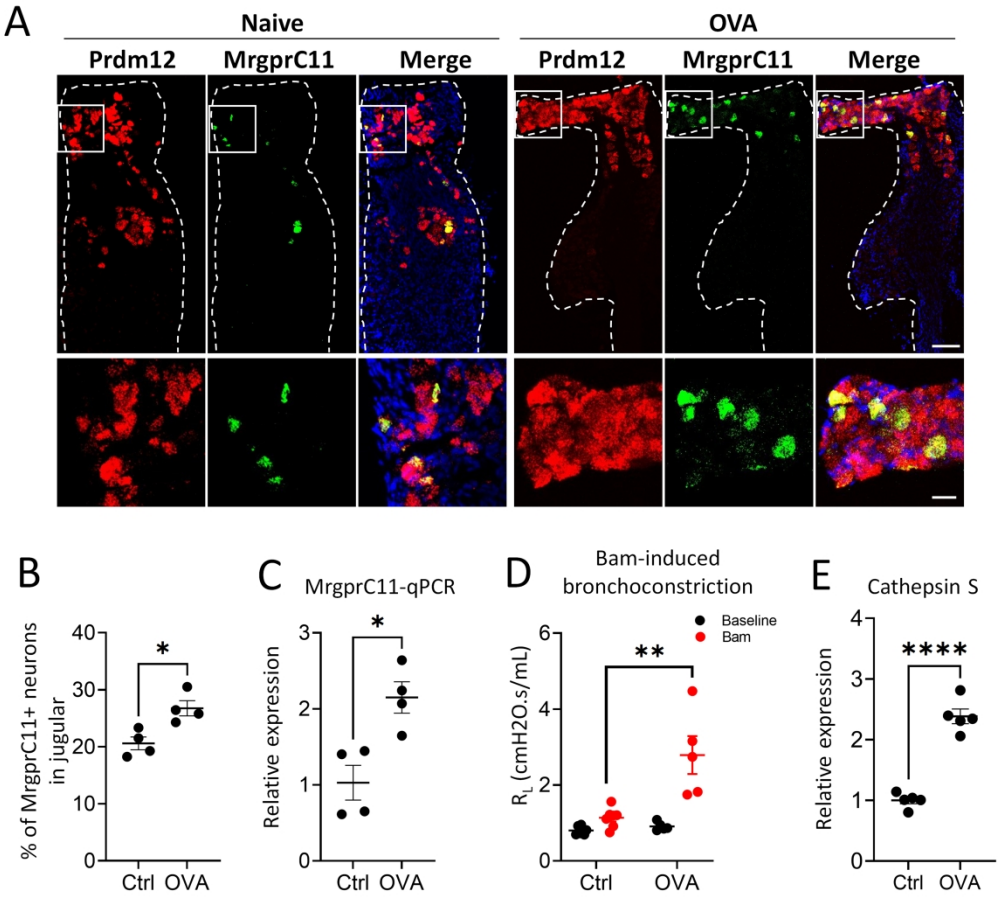

Figure 6. Allergic airway inflammation sensitizes MrgprC11+ jugular neurons. (A-B) RNAscope in situ showing the increased percentage of MrgprC11+ neurons in jugular neurons in asthmatic mice. Representative images of vagal ganglia sections from naïve and OVA-treated mice are shown in (A). The boxed areas in the upper panels are shown at greater magnification in the lower panels. The average percentages of MrgprC11+ neurons in jugular ganglia are shown in B. DAPI-nuclei stain was shown in blue in A. (C) Real time PCR analysis showing increased MrgprC11 mRNA level in vagal ganglia in inflamed mice. (D) Bam8-22-induced bronchoconstriction was also significantly increased in the inflamed mice. (E) Real time PCR analysis showing increased cathepsin S expression level in the inflamed lung. Welch's t-test for B, C, and E. Two-way ANOVA for D. *p < 0.05, **p < 0.01, ****p < 0.0001. Scale bars: A top panel , 100 μm, lower panel, 25 μm.

394x359mm (300 x 300 DPI)

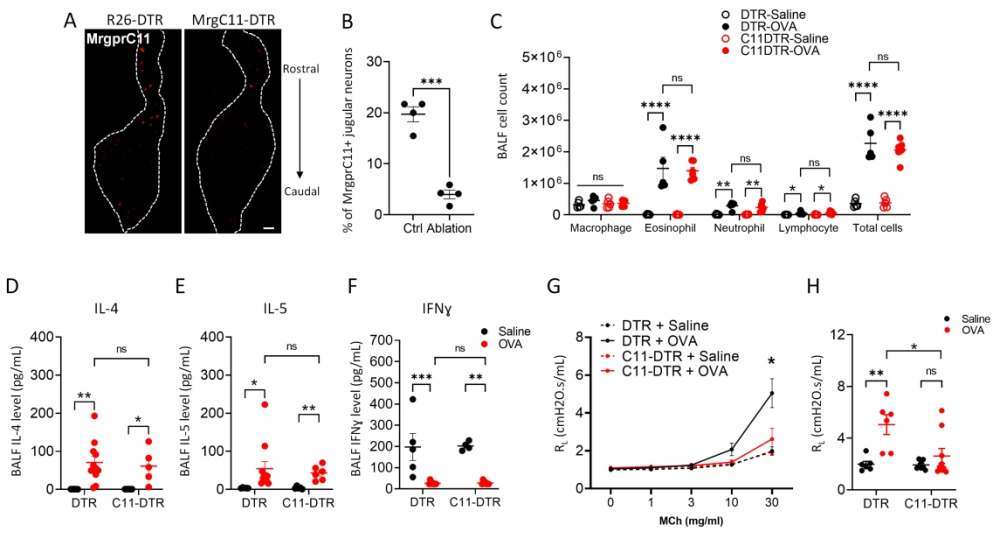

Figure 7. Ablation of MrgprC11+ jugular neurons blocked AHR. (A-B) MrgprC11+ neurons were ablated in DTX-treated MrgprC11DTR mice. Scale bars 50 μm. (C-F) Ablation of MrgprC11+ neurons did not affect the inflammatory cell count in BALF (C) and the level of IL-4 (D), IL-5 (E), and IFNɣ (F). (G) Ablation of MrgprC11+ neurons blocked airway hyperresponsiveness. Data collected for the 30 mg/ml MCh was replotted in dot plot in (H) to better visualize the differences between the control and cell ablation groups. Two-way ANOVA *p < 0.05, **p < 0.01. Scale bars: A, 100 μm.

670x362mm (200 x 200 DPI)

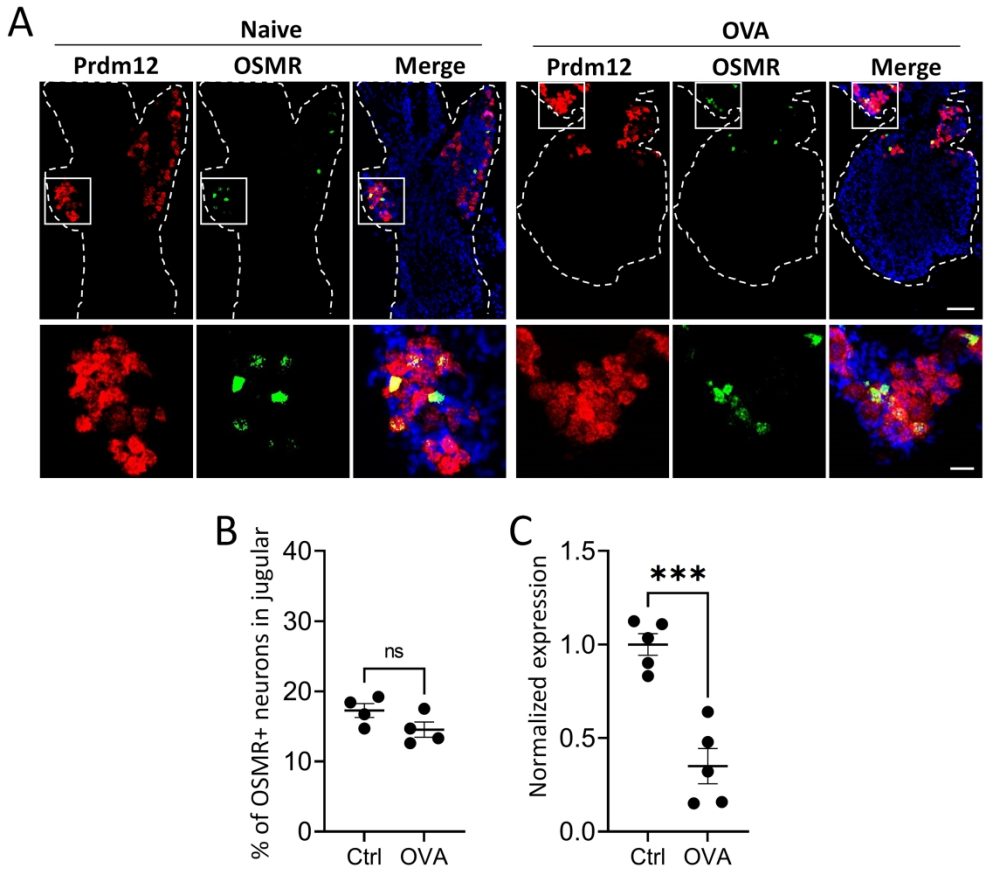

Figure S1. Expression of OSMR in jugular ganglia in naïve and OVA-treated mice. (A) RNAscope in situ showing the expression of OSMR and Prdm12 in naïve and asthmatic mice. The boxed areas in the upper panels are shown at greater magnification in the lower panels. DAPI-nuclei stain was shown in blue. (B) The percentages of OSMR+ neurons in jugular are comparable in naïve mice and asthmatic mice. (C) qPCR analysis of vagal ganglia showing that OSMR expression is decreased in the vagal sensory neurons in the inflamed mice. Scale bars: A top panel , 100 μm, lower panel, 25 μm.

413x367mm (300 x 300 DPI)

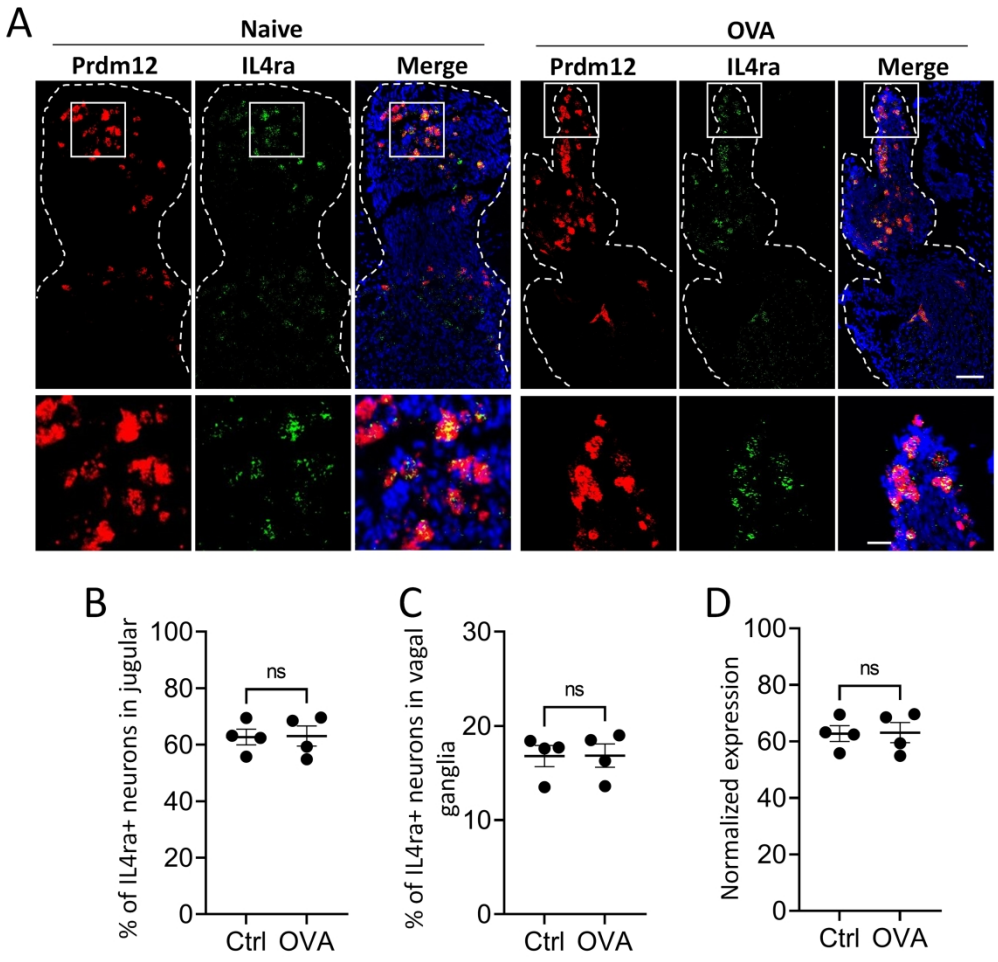

Figure S2. Expression of IL4ra in naïve and OVA-treated mice. (A) RNAscope in situ showing the expression of IL4ra and Prdm12 in vagal ganglia from naïve and asthmatic mice. The boxed areas in the upper panels are shown at greater magnification in the lower panels. DAPI-nuclei stain was shown in blue. (B) The percentages of IL4ra+ neurons in the jugular ganglia are comparable in naïve mice and asthmatic mice. (C) The percentages of IL4ra+ neurons in the vagal ganglia are comparable in naïve mice and asthmatic mice. (D) qPCR analysis of vagal ganglia showing comparable expression of IL4ra in naïve and inflamed mice. Welch's t-test. Scale bars: A top panel , 100 μm, lower panel, 25 μm.

400x386mm (300 x 300 DPI)

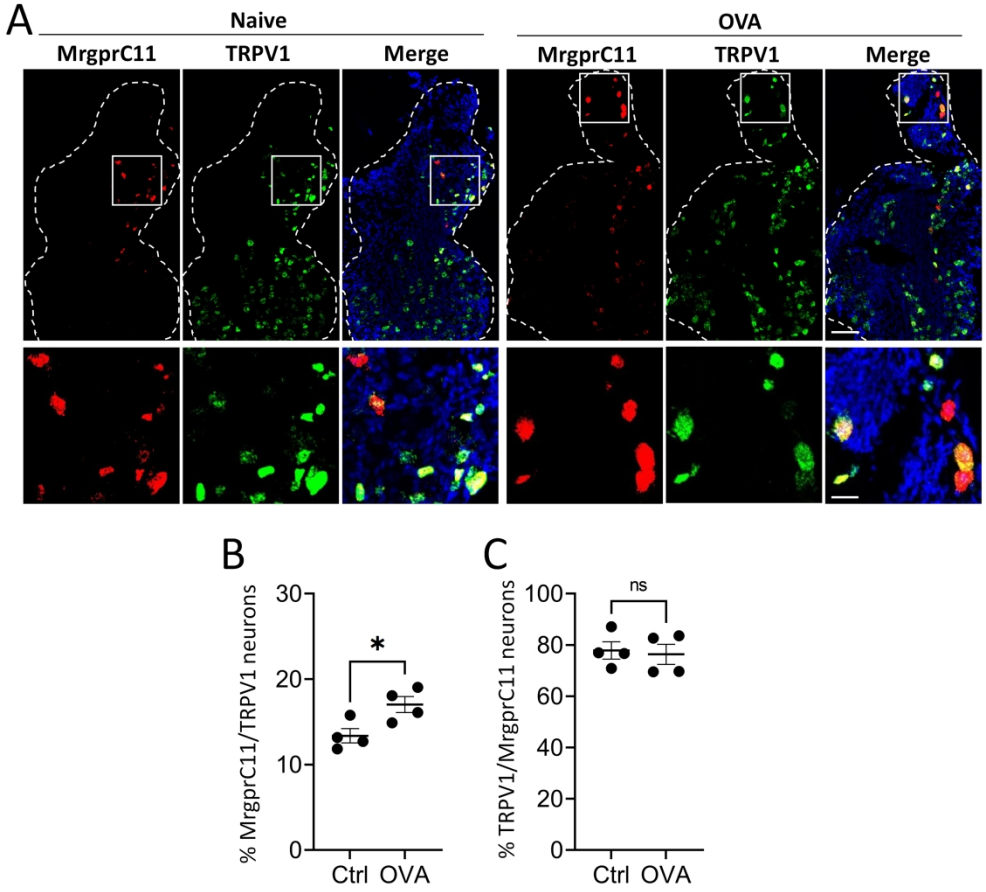

Figure S3. Expression of TRPV1 and MrgprC11 in naïve and OVA-treated mice. (A) RNAscope in situ showing the expression of TRPV1 and MrgprC11 in vagal ganglia from naïve and asthmatic mice. The boxed areas in the upper panels are shown at greater magnification in the lower panels. DAPI-nuclei stain was shown in blue. (B) The percentages of TRPV1+ neurons expressing MrgprC11 is increased in OVA-treated mice. (C) The percentages of MrgprC11+ neurons expressing TRPV1 are comparable in naïve mice and asthmatic mice. Welch's t-test for B. *p < 0.05. Scale bars: A top panel , 100 μm, lower panel, 25 μm.

435x392mm (300 x 300 DPI)